Synthesis and characterization of the anticancer and metal binding properties of novel pyrimidinylhydrazone derivatives

Veronika F.S. Pape[a,b], Dóra Türk[a], Pál Szabó[c], Michael Wiese[b], Eva A. Enyedy[d,*], Gergely Szakács[a,*]

[a] *Institute of Enzymology, Research Centre for Natural Sciences, Hungarian Academy of Sciences, Magyar Tudósok körútja 2, H-1117 Budapest, Hungary*

[b] *Department of Pharmaceutical Chemistry, University of Bonn, An der Immenburg 4, D-53121 Bonn, Germany*

[c] *Institute of Organic Chemistry, Research Centre for Natural Sciences, Hungarian Academy of Sciences, Magyar Tudósok körútja 2, H-1117 Budapest, Hungary*

[d] *Department of Inorganic and Analytical Chemistry, University of Szeged, Dóm tér 7. H-6720 Szeged, Hungary*

Keywords: Stability Constants · Metal Complexes · Arylhydrazones · Multidrug Resistance · Reactive Oxygen Species

* Corresponding authors: enyedy@chem.u-szeged.hu (E. A. Enyedy), szakacs.gergely@ttk.mta.hu (G. Szakács)

Abstract

Three novel pyrimidinylhydrazones substituted at either the aromatic moiety or at the imine carbon atom were synthesized and characterized by standard analytical methods. All compounds were found to be toxic in the micro- to submicromolar range against a diverse panel of cancer cell lines including multidrug resistant (MDR) derivatives expressing P-glycoprotein (Pgp). Using UV-visible spectrophotometry experiments demonstrated that the most active compound (**3**) forms highly stable complexes with iron(III) and copper(II) in a wide pH range with a stronger preference towards iron(III). The redox activity of the iron and copper complexes of ligand **3** was investigated using cyclic voltammetry and was tested with cellular reductants. The impact of reactive oxygen species (ROS) in the mechanism of toxicity was assessed using the ROS-sensitive cell permeable dye 2′,7′-dichlorofluorescin diacetate (DCFDA). Our results demonstrate that the studied pyrimidinylhydrazones form redox-active iron and copper complexes that are capable of producing intracellular ROS, which might lead to cellular damage and cell death in cancer cells regardless of their resistance status.

1. Introduction

The cellular homeostasis of metals is tightly regulated. As a result, only a minor fraction of the intracellular pools is freely available, and the majority of metal ions are bound to storage proteins or enzymes that utilize them as cofactors or as structural support elements [1,2]. It is estimated that at least one third of the human proteome consists of metalloproteins, many of which have been associated with various pathological conditions including infectious, cardiovascular and neurodegenerative diseases [3,4]. As compounds that can directly target the metal ion cofactors of metalloproteins are expected to have a significant biological effect, the development of chelators is a promising strategy in medicinal chemistry. Chelators have been traditionally used for the treatment of metal overload and diseases related to imbalanced metal homeostasis including hemochromatosis, β-thalassemia, and Alzheimer's or Parkinson's diseases [5,6]. Several studies have described the deregulation of iron homeostasis in cancer, suggesting that the altered metal homeostasis of cancer cells represents a vulnerability that can be targeted by chelation strategies [7,8]. Cancer cells increasingly rely on iron due to the crucial role of metalloproteins in proliferation. Since metal homeostasis is tightly linked to the regulation of the intracellular redox balance, anticancer metal complexes can also target cancer cells by the formation of redox active complexes giving rise to reactive oxygen species (ROS) [5,8].

Examples for chelators with antitumor potential include aroyl- and arylhydrazones, and variously substituted thiosemicarbazones [9–15]. The proposed mechanism of action of these antibacterial and anticancer compounds is based on the inhibition of the iron-requiring enzyme ribonucleotide reductase (RR) [5,8], the rate determining enzyme supplying deoxyribonucleotides for DNA synthesis [16]. The mammalian enzyme consists of two subunits: R1 harbours the catalytically active center; R2 contains a tyrosyl radical and a

diiron center [17]. Compounds targeting RR include antimetabolites such as gemcitabine, scavengers of the tyrosyl radical (hydroxyurea), gallium(III) complexes and various chelators. Triapine, a tridentate α-*N*-pyridyl thiosemicarbazone is a potent RR inhibitor currently undergoing phase I and II clinical trials [18–20]. Unfortunately, Triapine is subject to multidrug resistance (MDR), as it is recognized by the ATP-binding cassette (ABC) transporter P-glycoprotein (Pgp/ABCB1) [21]. MDR is a major obstacle in the treatment of cancer. Hence, there is an urgent need for new strategies aiming to overcome MDR [22]. Numerous metal complexes have been developed with the aim of bypassing or even targeting MDR, while minimizing the deplorable range of side effects of clinically used platinum complexes [23].

Arylhydrazones represent a promising chelator class characterized by antibacterial, antimycobacterial, analgesic and anticancer activities [12,13,24,25]. Several pyridyl- and pyrimidinylhydrazones were reported to be effective against multidrug resistant strains of leprosy and tuberculosis [13,26] and cancer cell lines [14]. Compared to closely related derivatives, pyrimidinylhydrazones with 4'-methoxy- and 5-ethyl-substituents have been suggested to show a higher and broader activity against Mycobacteria [15]. In the case of structurally related aroylhydrazones the introduction of an additional pyridine ring at the imine carbon of pyridylcarboxaldehyde isonicotinoyl hydrazone (PCIH) led to increased iron chelation and enhanced antitumor activity [11]. Here we have investigated the antitumor activity of arylhydrazones from the pyrimidinyl type. Since the α-position to the hydrazine moiety was shown to influence toxicity, we synthesized a derivative with methylation at the imine carbon. The ligands were tested for their *in vitro* antiproliferative activity in six human cancer cell lines. We show that three donor nitrogen atoms enable the formation of stable and redox-active complexes with iron(III) and copper(II). UV-visible (UV–Vis) spectrophotometric titrations were applied to investigate speciation in aqueous solution, and

cyclic voltammetry was used to characterize the redox activity of the complexes. The impact of metal ions on the antiproliferative activity and the formation of ROS was also investigated.

2. Materials and methods

2.1. Chemicals

Chemicals used for synthesis were procured from Acros Organics (Geel, Belgium), Alfa Aesar (Karlsruhe, Germany), Sigma-Aldrich (Schnelldorf, Germany) or TCI (Eschborn, Germany) and used without further purification. Column chromatography was performed using Silica gel 60 (40-63 μm, Merck, Darmstadt, Germany) as stationary phase. 3-(4,5-dimethylthiazol-2-yl)-2,5-diphenyltetrazolium bromide (MTT), N-acetylcysteine (NAC) and 2′,7′-dichlorofluorescin diacetate (DCFDA) were purchased from ABCR Chemicals (Karlsruhe, Germany), TCI (Eschborn, Germany) and Sigma Aldrich (Schnelldorf, Germany), respectively. The Pgp inhibitor WK-X-24 (XR9577) was used from prior synthesized stocks (Laboratory of Prof. M. Wiese, Bonn university, Germany) [27], Tariquidar was a kind gift from Dr. Susan Bates (NCI). Solid KOH, and tetrabutylammonium chloride (TBACl), ferrocene, uracil, 4-(2-hydroxyethyl)-1-piperazineethanesulfonic acid (HEPES), 2-(N-morpholino)ethanesulfonic acid (MES), ascorbic acid (ASC) and glutathione (GSH) were purchased from Sigma Aldrich and HCl, KCl, $CuCl_2$, $FeCl_3$ were Reanal products (Budapest, Hungary). Fe(III) and Cu(II) stock solutions were prepared by dissolving the appropriate amount of the metal chlorides in known amounts of HCl. Their concentrations were determined by complexometry via the EDTA complexes. Accurate strong acid content

of the metal stock solutions were determined by pH-potentiometric titrations. Ligand **3** was dissolved in pure DMSO to obtain the stock solution (0.01 M).

2.2. Synthesis and physical measurements

The ligands were prepared following the synthetic route suggested by Seydel *et al.* with minor modifications [15]. ^{1}H NMR and ^{13}C NMR spectra were obtained on either a Bruker Advance 300 or 500 spectrometer, respectively. DMSO-d_6 or $CDCl_3$ were used as solvents. Standard pulse programs were applied. Chemical shifts are expressed in ppm values using the residual solvent peaks as internal standards (DMSO-d_6 2.50; 39.52 ppm or $CDCl_3$ 7.26; 77.16 ppm) [28]. ^{13}C NMR signals were assigned with the aid of attached proton test (APT) spectra. Elemental analyses of the final products were performed on a Vario EL elemental analyser (Hanau, Germany). The values for carbon, nitrogen and hydrogen are given in percentage. Electrospray ionisation-mass spectrometry (ESI-MS) measurements for the characterization of the final products were carried out with a Waters Q-TOF Premier instrument (Waters Kft., Hungary) operating in positive ion mode; the samples were dissolved in methanol.

2.2.1. 4-Chloro-6-methoxypyrimidine

To a cooled solution (-10 °C) of 4,6-dichloropyrimidine (1193-21-1, 5 g, 33.56 mmol) in dry methanol, one equivalent of sodium hydride (titrated solution in dry methanol) was added, the solution was allowed to warm to room temperature and react for 48 h (depicted in *step a* of Scheme 1). The solvent was removed; the crude product was dissolved in brine, extracted with $CHCl_3$, and was used without further purification. ^{1}H NMR (500 MHz, DMSO-d_6): δ = 8.68 (d, ^{5}J(H,H) = 0.8 Hz, 1H, *H-2*), 7.18 (d, ^{5}J(H,H) = 0.9 Hz, 1H, *H-5*), 3.96 (s, 3H, OCH_3).

2.2.2. 4-Hydrazinyl-6-methoxypyrimidine

To a solution of the 4-chloro-6-methoxypyrimidine, obtained as described in 2.2.1., (2.5 g crude product) in methanol an aqueous solution of hydrazine (80%, 6.1 mL) was added and refluxed (see *step b* of Scheme 1). After evaporation of the solvent, the aqueous solution of the crude product was alkalized with NaOH and extracted with methylene chloride to give the product as an ochre powder in 60% yield. ^{1}H NMR (500 MHz, $CDCl_3$): δ = 8.26 (s, 1H, *H-2*), 6.42 (bs, 1H, N*H*), 6.07 (s, *H-5*), 3.92 (s, 3H, O*CH*$_3$), 3.42 (bs, 2H, N*H*$_2$). ^{13}C NMR (126 MHz, $CDCl_3$): δ = 170.72 (*C-6*), 167.17 (*C-4*), 157.68 (*C-2*), 84.90 (*C-5*), 53.87 (OCH_3).

2.2.3. 5-Ethyl-2-methyl-pyridine-N-oxide

35 mL of hydrogen peroxide (35% solution, 0.41 mol) was added to a solution of 5-ethyl-2-methyl-pyridine (104-90-5, 21.76 mL, 0.17 mol) in glacial acetic acid (200 mL) and refluxed for 16 h (depicted in *step c* of Scheme 1). After evaporation of the majority of the solvent, the reaction mixture was neutralized with NaOH and Na_2CO_3 and the starting material was retrieved by extraction with petroleum ether. 5-Ethyl-2-methyl-pyridine-*N*-oxide was extracted from the aqueous phase with $CHCl_3$, dried over Na_2SO_4 and after removal of the solvent obtained as a bright yellow liquid in 99% yield. ^{1}H NMR (500 MHz, $CDCl_3$): δ = 8.14 – 8.09 (m, *H*-6), 7.12 (d, ^{3}J(H,H) = 7.9 Hz, *H*-3), 7.00 (dd, ^{4}J(H,H) = 1.3 Hz, ^{3}J(H,H) = 7.9 Hz, *H*-4), 2.55 (q, ^{3}J(H,H) = 7.7 Hz, 2H, $C\underline{H_2}CH_3$), 2,48 (s, 3H, *CH*$_3$), 1.20 (t, ^{3}J(H,H) = 7.7 Hz, 3H, $CH_2C\underline{H_3}$).

2.2.4. 5-Ethylpyridin-2-yl-methyl acetate

As depicted in *step d* of Scheme 1, a solution of the 5-ethyl-2-methyl-pyridine-*N*-oxide, obtained in 2.2.5., (22.28 g, 0.16 mol) and acetic anhydride (28 mL, 0.23 mol) in glacial

acetic acid (7 mL) was refluxed for 3 h, put on ice, neutralized, extracted with methylene chloride. After removal of the solvent, the extract was dissolved in diethyl ether, washed with a saturated solution of Na_2CO_3 and dried over Na_2SO_4 to give the product in 85% yield. ^{1}H NMR (500 MHz, $CDCl_3$): δ = 8.42 (d, ^4J(H,H) = 2.1 Hz, *H*-6), 7.50 (dd, ^4J(H,H) = 2.2 Hz, ^3J(H,H) = 7.9 Hz, *H*-4), 7.24 (d, ^3J(H,H) = 7.9 Hz, *H*-3), 5.16 (s, 2H, *H*-7), 2.63 (q, ^3J(H,H) = 7.6 Hz, 2H, CH_2CH_3), 2.11 (s, 3H, COC*H3*), 1.22 (t, ^3J(H,H) = 7.6 Hz, 3H, CH_2CH_3). ^{13}C NMR (126 MHz, $CDCl_3$): δ = 170.79 (*C*=O), 153.04 (*C-2*), 149.35 (*C-6*), 138.70 (*C-5*), 136.11 (*C-4*), 121.89 (*C-3*), 66.98 ($\underline{C}H_2$-OAc), 25.89 ($\underline{C}H_2CH_3$), 21.01 ($CO\underline{C}H_3$), 15.36 ($CH_2\underline{C}H_3$).

2.2.5. 5-Ethylpyridin-2-yl-methanol

As depicted in *step e* of Scheme 1, 5-Ethylpyridin-2-yl-methyl acetate (24.29 g, 0.14 mol) was dissolved in tetrahydrofuran (THF) and refluxed with an aqueous solution of NaOH (8.1 g, 0.20 mol) for 5 h. The reaction mixture was reboiled on activated charcoal and was neutralized with glacial acetic acid and filtered. After concentration of the crude product under reduced pressure, it was dissolved in a saturated solution of $NaHCO_3$, extracted with diethyl ether and dried over sodium sulphate to give the product as a brown oil in 80% yield. ^{1}H NMR (500 MHz, $CDCl_3$): δ = 8.32 (d, ^4J(H,H) = 1.9 Hz, *H-6*), 7.48 (dd, ^4J(H,H) = 2.2 Hz, ^3J(H,H) = 7.9 Hz, *H-4*), 7.20 (d, ^3J(H,H) = 7.9 Hz, *H-3*), 4.70 (s, 2H, $C\underline{H_2}OH$), 2.60 (q, ^3J(H,H) = 7.6 Hz, 2H, $C\underline{H_2}CH_3$), 1.20 (t, ^3J(H,H) = 7.6 Hz, 3H, $CH_2C\underline{H_3}$). ^{13}C NMR (126 MHz, $CDCl_3$): δ = 157.10 (*C-5*), 148.12 (*C-6*), 137.99 (*C-2*), 136.34 (*C-4*), 120.55 (*C-3*), 64.29 ($\underline{C}H_2OH$), 25.81 ($\underline{C}H_2CH_3$), 15.40 ($CH_2\underline{C}H_3$).

2.2.6. 5-Ethylpicolinaldehyde

As depicted in *step f* of Scheme 1, MnO_2 was prepared freshly by simultaneously adding a solution of $MnSO_4$ hydrate (14.5 g, 0.09 mol in 25mL water) and NaOH (7.6 g, 2.21 mol in 20 mL water) to a warm solution of $KMnO_4$ (15.5 g, 0.10 mol in 100 mL water), refluxing the mixture for 6 h, filtered and dried under reduced pressure. 5-Ethylpyridin-2-yl-methanol (12.82 g, 93.4 mmol) was dissolved in chloroform and given to the dried MnO_2 (16.24 g, 186.8 mmol). The mixture was refluxed in an ultrasonic bath for 5 days, filtered and purified with column chromatography using a mixture petroleum ether and ethyl acetate (4:1) on silica gel to give the product as a bright yellow liquid in 61% yield. ^{1}H NMR (500 MHz, $CDCl_3$): δ = 10.03 (s, 1H, C*H*O), 8.60 (d, ^4J(H,H) = 1.9 Hz, *H-6*), 7.87 (d, ^3J(H,H) = 8.0 Hz, *H-3*), 7.70 – 7.63 (m, *H-4*), 2.73 (q, ^3J(H,H) = 7.6 Hz, 2H, C$\underline{H_2}$CH$_3$), 1.28 (t, ^3J(H,H) = 7.6 Hz, 3H, CH$_2$C$\underline{H_3}$). ^{13}C NMR (126 MHz, $CDCl_3$): δ = 193.30 (*C*HO), 151.06 (*C-2*), 150.18 (*C-6*), 144.67 (*C-5*), 136.28 (*C-4*), 121.72 (*C-3*), 26.43 ($\underline{C}$H$_2$CH$_3$), 15.02 (CH$_2\underline{C}$H$_3$).

2.2.7. Pyrimidinylhydrazones: ***1****, **2** and **3***

The three Schiff bases **1**, **2** and **3** were obtained by adding an ethanolic solution of the hydrazinyl component to the solution of the keto component in equimolar amounts (*step g* of Scheme 1), refluxing the mixture in the presence of catalytic amounts of acetic acid and recrystallization from aqueous ethanol.

2.2.7.1. 4'-Methoxy-6'-(2-(pyridin-2-ylmethylene)hydrazinyl)pyrimidine **(1)**

The reaction of 2-pyridinecarboxaldehyde (191.1 mg, 1.78 mmol) with 4-hydrazinyl-6-methoxypyrimidine (250 mg, 1.78 mmol) resulted in bright rosy crystals of the product in 72% yield (293 mg, 1.28 mmol). ^{1}H NMR (300 MHz, $CDCl_3$): δ = 8.78 (bs, N*H*), 8.60 (d, ^3J(H,H) = 4.8 Hz, *H-6*), 8.38 (d, ^5J(H,H) = 0.6 Hz, *H-2'*), 8.00 (d, ^3J(H,H) = 8.0 Hz, *H-3*), 7.93 (s, 1H, C=N*H*), 7.75 (t, ^3J(H,H) = 7.3 Hz, *H-4*), 6.63 (d, ^5J(H,H) = 0.7 Hz, *H-5'*), 3.99

(s, 3H, O*CH*$_3$). ^{13}C NMR (126 MHz, DMSO-d$_6$): δ = 170.00 (*C-4'*), 162.78 (*C-6'*), 157.77 (*C-2*), 153.47 (*C-2*), 149.28 (*C-6*), 142.77 (H*C*=N), 136.59 (*C-4*), 123.62 (*C-5*), 119.44 (*C-3*), 85.38 (*C-5'*), 53.54 (O*C*H$_3$). ESI-MS: m/z Calcd. for [M]: 229.0964. Found: 230.0979 for [M+H]$^+$, 252.0798 for [M+Na]$^+$. Anal. Calcd. for $C_{11}H_{11}N_5O\times0.75\ H_2O$: C, 54.43; H, 5.19; N, 28.85. Found: C, 54.36; H, 4.49; N, 28.94.

2.2.7.2. 4'-[2-[(5-Ethylpyridin-2-yl)methylidene]hydrazin-1-yl]-6'-methoxypyrimidine **(2)**

The reaction of 5-ethylpicolinaldehyde (241.1 mg, 1.78 mmol) with 4-hydrazinyl-6-methoxypyrimidine (250 mg, 1.78 mmol) resulted in bright rosy crystals of the product in 63% yield (288.7 mg, 1.12 mmol). ^{1}H NMR (500 MHz, DMSO-*d*$_6$): δ = 11.45 (s, 1H, N*H*), 8.43 (d, ^{4}*J*(H,H) = 1.6 Hz, *H-6*), 8.33 (d, ^{5}*J*(H,H) = 0.9 Hz, *H-2'*), 8.12 (s, C=N*H*), 7.93 (d, ^{3}*J*(H,H) = 8.1 Hz, *H-3*), 7.68 (dd, ^{4}*J*(H,H) = 2.1 Hz, ^{3}*J*(H,H) = 8.2 Hz, *H-4*), 6.49 (d, ^{5}*J*(H,H) = 0.6 Hz, *H-5'*), 3.89 (s, 3H, O*CH*$_3$), 2.64 (q, ^{3}*J*(H,H) = 7.6 Hz, 2H, C*H*$_2$CH$_3$), 1.20 (t, ^{3}*J*(H,H) = 7.6 Hz, 3H, CH$_2$C*H*$_3$). ^{13}C NMR (126 MHz, DMSO-*d*$_6$): δ = 169.96 (*C-6'*), 162.78 (*C-4'*), 157.74 (*C-2'*), 151.22 (*C-2*), 148.73 (*C-6*), 142.91 (H*C*=N), 139.16 (*C-5*), 135.87 (*C-4*), 119.11(*C-3*), 85.26 (*C-5'*), 53.50 (O*C*H$_3$), 25.15 (*C*H$_2$CH$_3$), 15.08 (CH$_2$*C*H$_3$).ESI-MS: m/z Calcd. for [M]: 257.1277. Found: 258.1272 for [M+H]$^+$, 280.1074 for [M+Na]$^+$. Anal. Calcd. for $C_{13}H_{15}N_5O$: C, 60.69; H, 5.88; N, 27.22. Found: C, 60.32; H, 5.76; N, 27.28.

2.2.7.3. 4'-Methoxy-6'-(2-(1-(pyridin-2-yl)ethylidene)hydrazinyl)pyrimidine **(3**, *VP035*)

The reaction of 2-acetylpyridine (0.2 mL, 1.78 mmol) with 4-hydrazinyl-6-methoxypyrimidine (250 mg, 1.78 mmol) resulted in bright rosy crystals of the product in 79% yield (342 mg, 1.41 mmol). ^{1}H NMR (500 MHz, DMSO-*d*$_6$): δ = 10.43 (s, 1H, N*H*), 8.57 (ddd, ^{5}*J*(H,H) = 0.9 Hz, ^{4}*J*(H,H) = 1.7 Hz, ^{3}*J*(H,H) = 4.8 Hz, *H-6*), 8.37 (d, ^{5}*J*(H,H) = 0.9 Hz, *H-2'*), 8.15 (dt, ^{5}*J*(H,H) = 0.9 Hz, ^{3}*J*(H,H) = 8.1 Hz, *H-3*), 7.85 – 7.75 (m, *H-4*), 7.35

(ddd, ^4J(H,H) = 1.1 Hz, ^3J(H,H) = 4.8 Hz, ^3J(H,H) = 7.4 Hz, 1H, *H-5*), 6.57 (d, ^5J(H,H) = 0.9 Hz, 1H, *H-5'*), 3.89 (s, 3H, OC*H*$_3$), 2.40 (s, 3H, C=NC*H*$_3$). ^{13}C NMR (126 MHz, DMSO-d_6): δ = 170.04 (*C-4'*), 163.51(*C-6'*), 157.53 (*C-2'*), 155.24 (*C-2*), 148.42 (*C-6*), 147.91 (*C*=N), 136.44 (*C-4*), 123.40 (*C-5*), 119.93 (*C-3*), 86.10 (*C-5'*), 53.50 (OCH$_3$), 11.76 (C=NCH$_3$). ESI-MS: m/z Calcd. for [M]: 243.1120. Found: 244.1128 for $[M+H]^+$, 266.0953 for $[M+Na]^+$. Anal. Calcd. for $C_{12}H_{13}N_5O\times0.5\ H_2O$: C, 57.13; H, 5.59; N, 27.76. Found: C, 57.23; H, 5.46; N, 27.09.

2.3. Determination of relative lipophilicity by HPLC

HPLC-MSMS measurements were run on an AB Sciex 3200 QTrap tandem mass spectrometer equipped with TurboV ion source. The injected mixture (5 µL) contained **1**, **2**, **3** and uracil at a concentration of about 1 µg/mL. The mass spectrometer was scanned in MRM mode; the Q1/Q3 transitions were as follows: **(1)** 230/105 and 230/93; **(2)** 258/133 and 258/121; **(3)** 244/227 and 244/186; (uracil) 113/96 and 113/70. The source parameters were as follows: dwell time: 200 msec; collision energy: 25 eV; IS (spray voltage): 5000 V; source temperature: 450°C; curtain gas: 25 instrument unit; GS1: 40 instrument unit; GS2: 40 instrument unit. A Perkin Elmer Series 200 microLC system (consisting of a binary pump, an autosampler and a column oven) was used for separation. Gemini C18 110A 150 x 4.6 mm, 5 µm was used at 40°C. The mobile phases were: A: 20 mM ammonium formate at pH = 10 adjusted by ammonia (pH = 10 was selected based on the log D versus pH curve. At pH = 10, the compounds are present in neutral form, see 3.3); B: methanol. Flow rate was 1 mL/min. The retention times of the compounds were measured at 45, 50, 55, 60 and 65% methanol for the accurate determination of log k (retention factor). Data acquisition was stopped after the elution of the last sample. A 15 minute equilibration step was used prior to the start of the runs at each solvent composition.

The reduced retention time was calculated using the following equation: $k = (t_0-t)/t_0$. Uracil was used for the exact determination of t_0. The retention time of uracil was 2.2 min at each solvent composition. The log k values of the different eluent composition runs were expressed as the function of the methanol content of the eluent, and extrapolated to pure water for the determination of log Kw.

2.4. UV–Vis spectrophotometry

The pH-metric measurements for determination of the exact concentrations of HCl and KOH stock solutions used for the spectrophotometric titrations were carried out at 25.0 ± 0.1 °C in aqueous solutions containing 0.5% (v/v) DMSO and at an ionic strength of 0.20 M KCl in order to keep the activity coefficients constant. All the titrations were performed with carbonate-free KOH solutions of known concentration (0.10 M) in the presence of 0.1 M KCl. An Orion 710A pH-meter equipped with a Metrohm combined electrode (type 6.0234.100) and a Metrohm 665 Dosimat burette were used for the pH-metric titrations. The electrode system was calibrated to the pH = -log[H^+] scale by means of blank titrations (strong acid *vs.* strong base; HCl *vs.* KOH) according to the method suggested by Irving *et al.* [29]. The average water ionization constant, pK_{water}, is 13.76 ± 0.01 at 25 °C, which corresponds well to the literature data [30]. Samples were deoxygenated by bubbling purified argon for *ca.* 10 min prior to the measurements and argon was also passed over the solutions during further titrations.

A Hewlett Packard 8452A diode array spectrophotometer was used to record the UV–Vis spectra in the 200 - 800 nm interval. The path length was 1 cm. The spectrophotometric titrations were performed on samples of ligand **3** alone or with Fe(III) or Cu(II). The concentration of the ligand was usually 0.05 mM and the metal-to-ligand ratios

were 1:1 and 1:2 over the pH range between 2 and 11.5 at an ionic strength of 0.20 M (KCl) at 25.0 ± 0.1 °C. The initial volume of the samples was 10.00 mL. Measurements for 1:1 ligand-to-Fe(III) system were also carried out by preparing individual samples in which KCl was partially or completely replaced by HCl. pH values, varying in the range *ca.* 0.7-2.0, were calculated from the HCl content.

Protonation constants of ligand **3**, the stability constants of its metal complexes and the individual spectra of the species were calculated by the computer program PSEQUAD [31] and literature data were used for Fe(III) hydroxido species [32]. $\beta(M_pL_qH_r)$ is defined for the general equilibrium $pM + qL + rH \rightleftharpoons M_pL_qH_r$ as $\beta(M_pL_qH_r) = [M_pL_qH_r]/[M]^p[L]^q[H]^r$ where M denotes the metal ion and L the completely deprotonated ligand. The calculations were always made from the experimental titration data measured in the absence of any precipitate in the solution.

2.5. Electrochemical Studies

Cyclic voltammograms of the Fe(III) and Cu(II) complexes were determined at 25.0 ± 0.1 °C in 90% (v/v) DMSO-water solution containing 1.0 mM metal ion or 1 mM ligand **3** while the metal-to-ligand ratio was varied between 1:1-1:3. Ionic strength was 10 mM (TBACl). Measurements were performed on a conventional three-electrode system under argon atmosphere and a PC controlled Electrochemical Measurement System (EF 451). Samples were purged for 15 min with argon before recording the cyclic voltammograms. A glassy carbon electrode was used the working electrode, a platinum electrode as the auxiliary electrode and Ag/AgCl/KCl (1 M) as reference electrode.

Electrochemical potentials were converted into the normal hydrogen electrode (NHE) scale by adding 0.236 V [33]. The electrochemical system was calibrated with a solution of

ferrocene in 90 % (v/v) DMSO-water ($E_{1/2}$ = +0.428 ± 0.012 V *vs.* Ag/AgCl/KCl (1 M) in our setup). Redox potentials were obtained at 100 mV/s scan rate in the range of –1.2 to +1.0 V.

2.6. Oxidation of ascorbic acid (ASC) and glutathione (GSH)

Oxidation of ASC and GSH by the copper(II) and iron(III) complexes of ligand **3** was studied by UV–Vis spectrophotometry using a Hewlett Packard 8452A diode array spectrophotometer. A special, tightly closed tandem cuvette (Hellma Tandem Cell, 238-QS, path length: 1 cm) was used and the reactants were separated until the reaction was triggered. Both isolated pockets of the cuvette were completely deoxygenated by bubbling a stream of argon for 10 min before mixing the reactants. Spectra were recorded before and immediately after mixing, and changes were followed for maximum 90 min. One of the isolated pockets contained the reducing agent (ASC or GSH) at ten times higher concentrations than that of the metal ions. The other pocket contained the metal ions (Cu(II): 25 μM; Fe(III): 50 μM) and ligand **3** at 1:1 metal-to-ligand ratio. The pH of the solutions was adjusted to 7.40 (copper complexes) or 5.45 (iron complexes) by 50 mM HEPES or MES buffers, respectively, and an ionic strength of 0.1 M (KCl) was applied at 25.0 ± 0.1 °C. At the end of the measurements *cc.* H_2O_2 (50 μL / 1.4 mL) was added to the samples.

2.7. Establishment of transgenic ABCB1 expressing Madin-Darby canine kidney II (MDCKII) cell line

MDCKII-ABCB1 cell line stably expressing the human wild-type MDR1/ABCB1 was established by the Sleeping Beauty transposon-based gene delivery system, using the 100x hyperactive SB transposase [34]. MDCKII canine kidney cells were cotransfected with the

SB transposon vector containing the wild-type human MDR1 cDNA [35] and the SB transposase vector construct, using the Lipofectamine 2000 reagent (Life Technologies) in accordance with the manufacturer's instructions. Briefly, 3×10^5 cells were seeded in 6-well-plates; 24 hours later the cells were transfected with 2 μg vector DNA per well in a 10:1 ratio for the SB transposon and transposase constructs. 48 hours after transfection transgene positive cells were sorted by flow cytometry (FACS Aria High Speed Cell Sorter, Beckton-Dickinson) based on the cell surface expression of wild-type and mutant MDR1/ABCB1. Protein expression was measured by antibody labeling using the human MDR1/ABCB1 specific monoclonal antibody MRK16 (Abnova). To obtain homogenous transgene positive cell population, sorting procedure was repeated 4 times in 2-week intervals.

2.8. Vector constructs

Sleeping Beauty transposon vector carrying the wild-type human MDR1 cDNA were constructed as follows. The Sleeping Beauty (SB) transposon vector containing the cDNAs of EGFP and the puromycin resistance gene (PURO) in separate transcription cassettes, each driven by CAG promoter, was kindly provided by Dr. Tamás István Orbán (Hungarian Academy of Sciences, Budapest, Hungary) [36]. Full-length wild-type MDR1 cDNA was amplified by PCR from pAcUW-LMDR1 vector [37] with the following primers: 5'-TAGAATACCGGTAGGTCGGAATGGATCTTGAA-3' and 5'-AGTGATGGATCCAACATCTCATACAGTCAGAG-3' containing AgeI and BamHI restriction sites, respectively. The digested PCR product was cloned into the SB-EGFP-PURO transposon vector between the AgeI and BclI restriction sites, replacing EGFP, resulting in SB-MDR1-PURO vector.

2.9. Cell culture

The human ovarian carcinoma cell lines A2780 and the doxorubicin selected multidrug resistant counterpart A2780adr were obtained from ECACC, UK, (A2780: No. 93112519, A2780adr: No. 93112520), and cultivated in RPMI (Sigma Aldrich, Germany) supplemented with 10% fetal bovine serum and 50 unit/mL penicillin and streptomycin (Sigma Aldrich, Germany). The human uterine sarcoma cell lines MES-SA and the doxorubicin selected MES-SA-Dx5 were obtained from ATCC (MES-SA: No. CRL-1976™, MES-SA-Dx5: No. CRL-1977™) and cultivated in Dulbecco's Modified Eagle Medium (DMEM, Sigma Aldrich, Hungary). The human cervix carcinoma cell line KB-3-1 and the vinblastine selected KB-v1 (kind gifts from Dr. Michael M. Gottesman, National Institutes of Health) were cultivated in DMEM. The phenotype of the resistant cells was verified using cytotoxicity assays (not shown). MDCK II and the Pgp transfected MDCK-B1 were cultured in DMEM. DMEM media (Sigma Aldrich, Hungary) were supplemented with 10% fetal bovine serum, 5 mmol/L glutamine, and 50 unit/mL penicillin and streptomycin (Life Technologies). All cell lines were cultivated at 37 °C, 5% CO_2.

2.10. MTT viability assay

MTT viability assays were performed as described earlier with minor modifications [38,39]. Briefly, cells were seeded into 96-well tissue culture plates (Sarstedt, Newton, USA / Orange, Braine-l'Alleud, Belgium) in the appropriate density evaluated for each cell line (5000 cells per well for MES-SA-Dx5 and KB-3-1/v1 cells, 10000 cells per well for A2780 cells) and allowed to attach for 12 h. Test compounds were added to achieve the required final concentration in a final volume of 200 µL per well. After an incubation period of 72 h, the

supernatant was removed and fresh medium supplemented with the MTT reagent (0.083 mg/mL) was added. Incubation with MTT at 37 °C was terminated after 1 h by removing the supernatants and lysing the cells with 100 µL DMSO per well. Viability of the cells was measured spectrophotometrically by absorbance at 540 nm using either a Perkin Elmer Victor X3 or a BMG POLARstar microplate reader. Data was background corrected by subtraction of the signal obtained from unstained cell lysates and normalized to untreated cells. Curves were fitted by Prism software [40] using the sigmoidal dose-response model (comparing variable and fixed slopes). Curve fit statistics were used to determine the concentration of test compound that resulted in 50% toxicity (IC_{50}).

2.11. ROS determination using DCFDA

Measurements were performed as reported in the literature with modifications [41–43]. After harvesting and washing with phosphate buffered saline (PBS), cells were incubated with 10 µM DCFDA in a water bath shaker at 37 °C for 30 min in a density of 3 Mio cells/mL. After washing with PBS cells were seeded to 96 well plates in PBS in a density of 20000 cells/well. Basal fluorescence was measured, after addition of the test compounds in different concentrations; samples were measured in time intervals of 10 min. DCFDA solution in buffer was used as a cell free control to test for interaction of the test compounds with DCFDA. Data was analysed as fold change of fluorescence compared to the basal levels.

3. Results and discussion

3.1. Synthesis

As depicted in Scheme 1, the pyrimidinylhydrazones **1** to **3** were prepared by reacting 4-hydrazinyl-6-methoxypyrimidine (derived from 4,6-dichloropyrimidine) with equimolar amounts of the respective keto component under mild acidic conditions. While compound **1** serves as the non-alkylated core structure, **2** possesses an ethyl group as substituent in the aromatic ring and **3** has a methylgroup at the imino carbon. 5-Ethylpicolinaldehyde used for the synthesis of **2** was prepared following the method patented by Seydel *et al.* in a slightly modified manner [15]. After formation of the N-oxide from 5-ethyl-2-methyl-pyridine using hydrogen peroxide in glacial acetic acid, followed by alkaline reconditioning, an acetoxy group was introduced using acetic anhydride, glacial acetic acid to provide 5-ethylpyridin-2-yl-methyl acetate. The cleavage of the ester to the corresponding alcohol was carried out in THF, as the suggested conditions using ethanol as a solvent provided the ethyl ether instead. The oxidation to the desired aldehyde required a long time; and reflux with freshly prepared MnO_2 under ultrasound was found to be an efficient oxidizing method. Several other methods including commercially available MnO_2 [15], the application of SeO_2 and tert-butyl hydroperoxide [44], or the attempt to directly oxidize the 5-ethyl-2-methyl-pyridine [45–47] were not successful. With the help of the modifications in the first and in the last steps of the original approach, the yield could be increased from the reported 18% to 40%.

Physico-chemical properties are known to influence pharmacokinetics and pharmacodynamics; therefore we were interested in the lipophilicity of the three compounds. Since the lipophilicity of the compounds was too high to allow the exact determination of $\log D_{7.4}$ values by the traditional shake flask method in *n*-octanol/buffered aqueous solution (1:1), $\log D_{7.4}$ values were estimated using MarvinSketch [48] and the relative lipophilicity of the compounds was determined using HPLC. This method is commonly used for the

determination of log K_w (log P) [49]. We used an isocratic method to measure the retention times of the neutral forms of the compounds as a function of the organic composition of the eluent. Results of five different eluent compositions (summarized in Supplementary Table A1) were used for the accurate determination of the log k values as described in the *Materials and Methods* section. Since in this setup the retention coefficients of the three analytes show linear correlation with the volume fractions of the organic solvent in the binary eluent, the relative lipophilicity of the compounds was determined using the linear solvent strength model ([49]). The resulting log K_w values are shown in Table 1.

*3.2. Characterizing the in vitro antitproliferative activity of compounds **1** to **3***

The cytotoxic potency of pyrimidinylhydrazones **1** to **3** was investigated in a diverse panel of cancer cell lines including A2780 (ovarian carcinoma cells), KB-3-1 (cervix carcinoma) and MES-SA (uterine sarcoma). To test the ability of the newly synthesized compounds to overcome drug resistance, resistant derivatives of the cell lines (A2780adr, KB-v1 and MES-SA- Dx5) were also included in the study. Resistance of these cell lines is primarily mediated by the overexpression of Pgp, which effluxes structurally and mechanistically unrelated cytotoxic compounds from the cells [50–52]. To clearly delineate the effect of Pgp on the toxicity of the compounds, we included control MDCK-II and its drug resistant derivative MDCK-II-ABCB1 engineered to overexpress cDNA-derived Pgp.

As summarized in Table 2, the three tested compounds proved to be toxic in all investigated cell lines (with IC_{50} values of 0.03 – 6.30 μM) regardless of their resistance status towards common cytostatic agents. Toxicity of the compounds does not correlate with lipohilicity (Table 1). Alkylation of **1** resulted in increased toxicity in all eight investigated cell lines.

Introduction of a methyl at the imino carbon, as in **3** increases toxicity to a higher extent as compared to the introduction of an ethyl group at the aromatic ring as in compound **2**.

3.3. Proton dissociation processes of ligand 3

Since the physico-chemical properties of a potential chemotherapeutic agent have a basic influence on its pharmacokinetics and metal binding abilities, a detailed study on the proton dissociation processes of the most promising compound **3** was performed. For this purpose UV–Vis spectrophotometric titrations were applied at a concentration of 50 μM (in the presence of 0.5% (v/v) DMSO). The recorded pH-dependent spectra (Fig. 1a) revealed two proton dissociation processes at pH < 9; the calculated protonation constants ($\log\beta(H_iL)$) and pK_a values are reported in Table 3. The spectra for the individual ligand species in different protonation forms (H_2L^{2+}, HL^+ and L) were calculated by the deconvolution of UV-Vis spectra recorded at different pH values (Fig. 1b). Titrations showed characteristic spectral changes in the wavelength range 250 – 450 nm. Ligand **3** displays an intense absorption band in all the protonation forms at 344 nm (H_2L^{2+}), 356 nm (HL^+) and 312 nm (L), and less intense bands at 276 nm (H_2L^{2+}) and 282 nm (HL^+), which are assigned to $n \rightarrow \pi^*$ transitions. The determined pK_a values demonstrate that the proton dissociation processes overlap and the neutral form L predominates in the physiological pH range as illustrated in Fig. 1c. pK_1 can most presumably be attributed to the deprotonation of the pyrimidinium unit, while pK_2 belongs to the deprotonation of the pyridinium-N as shown in Scheme 2. Deprotonation of the pyridinium moiety in the case of the α-N-pyridyl thiosemicarbazones such as the drug Triapine was also shown to result in similar spectral changes, namely a significant shift of λ_{max} value from 402 nm to 368 nm [53]. The possible proton dissociation

of the hydrazinic =N-N*H* group of ligand **3** is likely to take place at higher pH values (pH > 11) and therefore its pK_a could not be determined accurately with the applied method.

*3.4. Complex formation processes of ligand **3** with Fe(III) and Cu(II)*

The biological activity of metal binding compounds is often modified upon complex formation with metal ions [18,54]. Characterization of metal binding ability (solution speciation), and the most plausible chemical species formed in aqueous solution in the biologically relevant pH range is a mandatory prerequisite for understanding the mechanism of action of complexes. To this end, we determined the stoichiometry and stability of ligand **3** complexes formed with Fe(III) and Cu(II) in aqueous solutions using UV-Vis spectrophotometry. The stoichiometries of the metal complexes and the overall stability constants furnishing the best fits to the experimental data are listed in Table 4. The appearance of well-defined charge transfer (CT) bands in the visible wavelength range of pH-dependent UV–Vis spectra unequivocally showed complex formation with both metal ions (Figs. 2 and 3). These CT bands overlap considerably with the ligand bands, while the d-d bands are too weak to be detected under the concentrations conditions used (c_M = 25 - 50 μM). In the case of Fe(III), formation of the expected complexes $[FeL]^{3+}$ and $[FeL_2]^{3+}$ could be verified. In these complexes the ligand coordinates most probably via ($N_{pyridyl}$,$N_{hydrazone}$,$N_{pyrimidyl}$) donor sets. It is noteworthy that $[FeL_2]^{3+}$ is the predominant species at 1:2 metal-to-ligand ratio in the physiologically relevant pH range (see inset of Fig. 2), although the hydrolysis of the metal ion suppresses the complex formation at pH > 8.5. Surprisingly, the development of CT bands that are characteristic for Fe(II) complexes formed with ligands consisting of aromatic nitrogen donor atoms was also detected at pH >

~ 8.5 in the 510–610 nm wavelength range. Formation of minor amounts of iron(II) complexes is possible at lower pH values as well. The redox process of the complex seems to be pH-dependent and much faster in the basic pH range. Thus data collected at pH > 7.5 were not evaluated.

In order to compare the iron binding ability of ligand **3** with that of other well-known iron chelators, the pM value (= -log [Fe(III)]; c_L/c_M=10; c_M =1 μM) was calculated at physiological pH, using the experimentally determined stability constants. For Fe(III) a pM value of 17.6 was obtained, which is lower than those reported for the naturally occurring iron binders such as human serum transferrin (20.3) [55], desferrioxamine B (26.5) [56] or the chelator Deferiprone (19.3) used to treat thalassaemia major [57], but is higher than the pM value of the thiosemicarbazone drug Triapine (15.7) [58]. Since higher pM values imply that metal complex formation is more favored, these results suggest that the studied pyrimidinylhydrazone forms less stable complexes compared to the aforementioned chelators containing mainly oxygen donor atoms. However, the Fe(III) binding ability of ligand **3** can exceed that of the tridentate α-N-pyridyl thiosemicarbazones with a ($N_{pyridyl}$,N,S^-) binding mode at pH 7.4.

In the case of the Cu(II) ion, the formation of mono-ligand complexes was expected due to the usual square planar geometry of the Cu(II) coordination sphere, although the speciation model was significantly improved by the involvement of bis-ligand $[CuL_2]^{2+}$ species (see Fig. A1). Deconvolution of the UV–Vis spectra recorded in the Cu(II) – ligand **3** system yielded the formation constants summarized in Table 4; individual spectra of the $[CuLH]^{3+}$, $[CuL]^{2+}$ and $[CuL_2]^{2+}$ complexes are shown in Figs. 3b and A2. Formation of the bis-ligand Cu(II) complex is not as pronounced as in the case of Fe(III), which is reflected in the fact that its molar fraction is only 0.52 at pH 7.4 (c_L/c_M =2; c_L = 50 μM), while the corresponding value is 0.80 in the case of $[FeL_2]^{3+}$ under the same conditions. In the

protonated complex $[CuLH]^{3+}$ the ligand coordinates most probably in a bidentate manner (*i.e.* ($N_{pyridyl}$,$N_{hydrazone}$); in $[CuL]^{2+}$ via the tridentate mode ($N_{pyridyl}$,$N_{hydrazone}$,$N_{pyrimidyl}$) was suggested for pyridylhydrazones, which comprise similar binding moieties [59]. In case of the $[CuL_2]^{2+}$ species a distorted octahedral binding mode or a bidentate coordination of the ligands may be possible, which is difficult to ascertain without EPR studies.

In order to compare the Cu(II) and Fe(III) binding ability of ligand **3**, the pM value was also computed on the basis of the stability data (conditions: pH = 7.40; c_L/c_M = 10 μM; c_M = 1 μM) and a value of 8.6 was obtained for Cu(II). Since Fe(III) tends to hydrolyze at physiological pH, its hydroxido species were also taken into account and a modified pM value (pM*) was determined for Fe(III), by calculating the negative logarithm of the summed equilibrium concentrations of the free metal ion and its hydroxido species (pM* = -log ([Fe] + $\Sigma[Fe_p(OH)_r]$). pM* for Fe(III) was computed to be 9.5, which is almost one order of magnitude higher than the pM of Cu(II). At an acidic pH (5.45) pM* can be considered equal to pM, due to the lower extent of hydrolysis, therefore values of 8.5 and 13.3 were computed for the Cu(II) and Fe(III) complexes, respectively. These results indicate that whereas ligand **3** forms stable complexes with both Fe(III) and Cu(II), the unbound metal fraction is somewhat higher in the case of Cu(II) showing the stronger Fe(III) binding ability of ligand **3** under physiological conditions and in the slightly acidic pH range as well.

3.5. Effect of the metal ions on the toxicity of ligand 3

Having shown the strong metal binding ability of ligand **3** to Fe(III) and Cu(II), experiments were designed to evaluate the impact of metal ions on its toxicity. Ligand **3** was added to the parental MES-SA cells and its resistant derivative MES-SA-Dx5 with increasing

concentrations of metal ions. The metal salts alone had no impact on cell viability over a three day long incubation period; therefore additive effects could be excluded. In MES-SA cells, coincubation of **3** with Fe(III) was found to reduce the ligand's cytotoxicity, while the presence of Cu(II) had an opposite effect (Fig.4). Interestingly, the effects of both metal ions, namely the rescuing by iron and the sensitization by copper was found to be significantly attenuated in MES-SA-Dx5 cell line, the drug resistant derivative of MES-SA.

Reduced activity of the free ligand in the presence of the iron indicates that the toxicity may – at least in part – be explained by the depletion of cellular iron levels. The differential sensitivity of the drug resistant subline is reminiscent of the collateral sensitivity of MDR cells [60]. The mechanisms underlying the paradoxical hypersensitivity of resistant cells are not known. It has been suggested, but never shown, that the metal homeostasis of MDR cells is altered as a result of Pgp function. Lack of the protective effect of Fe(III) in the MDR subline suggests that these cells cannot be rescued by excess iron – perhaps due to the imbalanced iron homeostasis of MDR cells.

In follow up experiments the Cu(II) and Fe(III) complexes of ligand **3** were prepared *in situ* by mixing the ligand with half- and one equimolar concentrations of the metal ions. Using this setup a constant molar ratio was ensured throughout the investigated concentration range (1 nM – 250 μM). Results obtained in the presence of increasing metal ion concentrations at a fixed ligand-to-metal molar ratio confirmed the reduced toxicity of Fe(III) complexes (not shown), while the effect of Cu(II) was less pronounced in that setup as compared to the coincubation (Fig. 7).

*3.6. Cyclic voltammetric studies of Fe(III) and Cu(II) complexes of ligand **3***

Besides depleting metal ions, the mechanism of toxicity of chelating compounds also relies on redox active complexes that may be formed in the Fenton reaction [1,7,41]. To examine the redox properties of the iron and copper complexes of ligand **3**, we performed cyclic voltammetry (CV) studies and the measured formal potentials were compared to those of Triapine and physiological reductants. Illustrative voltammograms are shown in Fig. 5. Measurements were performed in 90% (v/v) DMSO/H_2O in the potential range of –0.9 to +1.0 V against Ag/AgCl/KCl (1 M). Ligand **3** alone was found to be redox-innocent in this range. It should be noted that the ligand alone shows an irreversible process resulting in a cathodic peak seen at ~ –1.01 V *vs.* Ag/AgCl/KCl (1 M) (which corresponds to –0.78 *vs.* NHE, Fig. A3). The complexes of both metal ions showed redox activity. The redox potential of the formed complexes is largely controlled by the donor atoms of the ligand that are present in the first coordination shell. The addition of the chelating agent significantly changed the peak positions in comparison to those of the aqua complexes. The detected redox processes for the Fe(III)/Fe(II) and Cu(II)/Cu(I) couples were found to be quasi reversible under the applied conditions in all cases. (For a detailed analysis of CV data see Table A2.)

Addition of ligand **3** to Fe(III) results in the formation of a metal complex and the appearance of a new set of peaks in the voltammograms at ~ +0.68 V *vs.* NHE as calculated from the measured data represented in Fig. 5a. Upon complexation the formal potential increased by 0.31 V; the intensity of the aqua ion peaks decreased, while that of the metal complex increased with increasing ligand excess. The positive shift of the formal potentials due to the coordination by the ligand via ($N_{pyridyl}$,$N_{hydrazone}$,$N_{pyrimidyl}$) donor set indicates a preference for the lower oxidation state, as in the case of other well-known ligands consisting of aromatic nitrogen donor atoms such as 2,2′-bipyridyl or 1,10-phenanthroline. This can be a possible explanation for the reduction of Fe(III) complexes in the basic pH range (*vide supra*).

The formal potential of the complexed Fe(III)/Fe(II) redox couple is significantly higher (~ +0.69 *vs.* NHE) than that of other iron chelators such as Triapine (+0.07 V *vs.* NHE) [58] or tris-hydroxamato complexes (-0.43 V) [61] resulting in an easier reduction by physiological reductants.

Ligand **3** also influences the redox potential of the Cu(II)/Cu(I) couple. Addition of the ligand diminished the intensity of the aqua complex peaks, while a new reduction peak appeared upon complexation. In case of the copper complexes, the formal potential was shifted by 0.25 V to the negative direction, indicating the ligand preference for the metal ion in the higher, +2 oxidation state. The formal potential of the Cu(II)/Cu(I) in the case of ligand **3** (+0.36 V *vs.* NHE) is higher than that of the biological reductants (glutathione, ascorbate [1,62]), thus the reduction of this Cu(II) complex may lead to redox cycling and the generation of ROS.

*3.7. Reduction of complexes formed with ligand **3** by intracellular reducing agents*

In order to further investigate the potential of the copper and iron complexes formed with ligand **3** to undergo intracellular redox reactions, the ability of biologically relevant reducing agents such as ascorbate (ASC) or glutathione (GSH) to reduce the complexes was tested in in vitro assays. The redox processes were followed spectrophotometrically under strictly anaerobic conditions *via* monitoring the overlapping ligand and CT bands in the wavelength range of 300-600 nm. Kinetic runs were performed at pH 7.40 in the case of the copper complexes, while pH 5.45 was chosen for the iron complexes in order to avoid metal ion hydrolysis and the possible formation of the Fe(II) species in the Fe(III) - ligand **3** system in the basic pH range (see Section 3.3). Oxidation of ASC yields dehydro-L-ascorbic acid; the

oxidized form of GSH is glutathione disulfide (GSSG). Neither the reduced and oxidized form of ASC nor GSH absorbs light at $\lambda > \sim 310$ nm [63], thus spectral changes above this wavelength are characteristic only to the absorption of the metal complexes. Oxidation of ASC or GSH is often monitored at their λ_{max} values (265 and 262 nm, respectively) [9,64], but since the studied metal complexes, as well as the free ligand **3** absorb light strongly in the UV range, the UV–Vis spectra were recorded between $\lambda \sim 300$ nm and 600 nm upon addition of ASC and are shown in Fig. 6. No time dependent spectral changes were observed (t_{max} = 75 min) in the case of the Cu(II) complexes (Fig. 6a), which suggests that this metal complex could not be reduced by ASC under the applied conditions.

We also monitored the spectral changes of the formed complexes upon reduction by GSH (Fig. 6c). Glutathione is a predominant intracellular reducing agent with a lower formal potential compared to that of ASC. (The formal potential at pH 7.4 of the GSSG/GSH and the dehydro-L-ascorbic acid/ASC redox pairs are -0.26 V and +0.05 V, respectively [62,65].) In the case of copper a significant decrease of the absorbance was observed at the λ_{max} value of the Cu(II) complex (408 nm) during the redox reaction; while the absorbance value was increased at the λ_{max} of the free ligand (~310 nm), most probably as a result of the decomposition of the generating instable Cu(I) complex. These results suggest that the stronger reducing agent GSH is able to reduce the Cu(II) complex. Addition of H_2O_2 regenerated the Cu(II) complexes, suggesting that a reversible redox process can contribute to the toxicity of the compound.

In line with the high redox potential of the Fe(III)-ligand **3** complex (see Section 3.6), this complex was reduced by ASC (Fig. 6 b); yet the redox reaction was relatively slow. When H_2O_2 was added to the sample at the end of the kinetic run only negligible spectral changes

were observed even after 0.5 h, suggesting that the iron complex is not likely to undergo intracellular redox cycling.

Surprisingly, ten-fold excess of GSH resulted in almost no changes in the UV–Vis spectrum of the Fe(III) - ligand **3** system (Fig. 6 b) within 90 min, suggesting that the kinetic of the reduction is fairly slow. A similar trend was observed in the reduction kinetics of vanadium complexes by the two reducing agents [63,64]. Furthermore, the formal potentials of both reducing agents are pH-dependent, which might also explain the lack of GSH-induced reduction of the iron complex at pH 5.45. Based on studies on the pH dependence of the redox potentials, it can be estimated that at pH 5.45, the redox potential of GSH and ASC are shifted by 116 mV and 52 mV, respectively [62,65,66]).

Taken together, our results indicate that the Cu(II) complex of ligand **3** has the potential to undergo redox-cycling reactions under physiological conditions, whereas the iron complex is probably not able to undergo intracellular redox cycling.

*3.8. Involvement of ROS in the toxicity of **3***

To evaluate the role of ROS production in the toxicity of **3**, the cytotoxicity experiments were repeated in the presence of the antioxidant NAC. Coincubation with NAC resulted in a significant increase of the IC_{50} values (Fig. 7), suggesting that ROS play a role in the toxicity of ligand **3**. Due to the relative redox potentials a direct reduction of compound **3** by NAC is unlikely; therefore a more probable source of ROS induction is the intracellular formation of redox active complexes undergoing Fenton-like chemistry. In the next set of experiments Cu(II) complexes of ligand **3** were coincubated at 1:1 and 1:2 metal-to-ligand ratios with NAC and cytotoxicity was measured in MES-SA and MES-SA-Dx5 cells. Since

complexation with Fe(III) significantly attenuates the toxicity of ligand **3**, the effect of NAC on the toxicity of the iron complexes could not be reliably determined.

As expected, NAC diminished the toxicity of the Cu(II) complexes, suggesting that ROS may, at least in part, be responsible for the toxicity of the ligand and its metal complexes (Fig. 7c). Intriguingly, the (relative) protective effect of the antioxidant appeared to be more pronounced in drug resistant cells as compared to their sensitive counterparts (compare A2780adr, Fig. 7b to A2780, Fig. 7a, and dx5 to MES-SA (Fig 7c)).

To characterize the extent of ROS formation, intracellular ROS were measured using the ROS-sensitive cell permeable dye DCFDA. MES-SA and MES-SA-Dx5 cells were preincubated with DCFDA and the effect of ligand **3** and its complexes on fluorescence was evaluated following an 80 minute-long incubation period. Fig. 8 summarizes the results obtained with MES-SA cells (Dx5 cells yielded similar results; Fig. A4). At 50 μM, ligand **3** did not induce an increase in fluorescence. Complexation with iron resulted in ROS production in the case of both metal-to-ligand ratios used ($[FeL]^{3+}$ and $[FeL_2]^{3+}$) (Fig. 8a). Addition of Cu(II) resulting in 1:1 metal-to-ligand ratio (mostly $[CuL]^{2+}$, see Fig. A2) induced the formation of ROS, while the $[CuL_2]^{2+}$ complex was not redox active (Fig. 8a). In all cases, ROS induced by the metal complexes could be scavenged by the addition of NAC. A similar pattern was observed at 100 μM ligand concentration (Fig. 8b). Unexpectedly, addition of the ROS scavenger NAC to 100 μM of the $[CuL]^{2+}$ complex increased, rather than decreased ROS production. Since this effect could also be observed in the cell free condition, we speculate that the paradoxical effect of NAC is explained by the ability of the complex to participate in redox cycling as a result of the reduction by NAC (see also Figures 5b, 6c). The Fenton-like reaction results in increased ROS production, but direct oxidation of DCFH may also contribute to the observed signal [67,68]. Induction of ROS by NAC was only observed at 100 μM ligand concentration, which is between 300 and 1000 times higher than the IC_{50}

values obtained in the toxicity studies displayed in Fig 7c. At $[CuL]^{2+} \leq 50$ μM, addition of NAC protects against the formation ROS (Fig. 8a), in line with the protective effect of NAC against the toxicity of compound **3** even in combination with copper (Fig. 7c).

3.9. Evaluation of the toxicity of ligand 3 in MDR cells

Chelators that bypass resistance mechanisms are promising candidates for anticancer drug development [8,69]. ABC transporters contribute significantly to the multifactorial phenomenon of MDR [70–72]. As a strategy to overcome Pgp-mediated MDR, several inhibitors have been developed [73,74]. Despite promising in vitro results, successful translation of MDR transporter inhibition to the clinic remains elusive [75–77]. Hence there is an urgent need for novel chemotherapeutics with marked and selective antitumor activity, particularly those that can overcome resistance to established therapies. Several chelators have been reported to overcome or even exploit MDR [8,69]. The toxicity pattern of the newly synthesized compounds, showing activity in micro- to submicromolar range in all investigated cell lines regardless of their resistance status (Table 2), suggests that these compounds are not susceptible to Pgp-mediated efflux. Interestingly, compound **3** shows enhanced activity towards the Pgp expressing MES-SA-Dx5 and A2780adr derivatives. Paradoxical toxicity towards otherwise resistant cells was observed in the case of several chelators, as for the thiosemicarbazone NSC73306 [69]. Intriguingly, the toxicity of the so-called MDR-selective compounds is increased, rather than attenuated by the activity of efflux transporters such as Pgp [60,69,78]. To determine the role of Pgp in the increased sensitivity of MDR cell lines to compound **3**, cytotoxicity measurements were repeated in the presence one of of the Pgp-inhibitors TQ or WK-X-24 (Fig. 9) [73,74]. Inhibition of Pgp did not

influence the toxicity of the compounds, suggesting that the observed hypersensitivity of the cells is linked to other factors than Pgp.

4. Conclusions

There is a continuous demand for the development of novel types of antitumor agents especially with the potential to overcome multidrug resistance. In this work three new pyrimidinylhydrazone Schiff bases were synthesized and characterized, and their antitumor potential and putative mechanisms of action were evaluated. The cytotoxicity of the compounds was studied in a panel of human cancer cell lines and the canine MDCK-ABCB1 that was explicitly engineered to evaluate the effect of Pgp, the ATP-dependent pump responsible for the efflux of a broad spectrum of cytotoxic agents. The three tested compounds proved to be cytotoxic in the micro- to submicromolar range, regardless of the resistance status of the cells. Methylation of the core structure at the imine carbon resulted in the most active compound among the studied derivatives (**3**), since it seemed to increase the toxicity to a higher extend than the introduction of an ethyl-substituent in the pyridine-moiety.

Due to the metal binding ability of ligand **3**, its biological activity is likely to be mediated via the formation of complexes with essential metal ions. The high stability of the Fe(III) complex together with a protecting effect upon coincubation with the metal ion suggests that the mechanism of action might be partly mediated by iron depletion. Also with Cu(II) stable complex formation could be observed. While the complexes of both metal ions show redox activity in cyclic voltammetry measurements, only the Cu(II) complex shows a reversible redox cycling in biological relevant conditions (GSH reduction followed by H_2O_2 oxidation).

The intracellular redox cycling of metal complexes might result in ROS formation (Fig. 10). A similar mechanism ("activation by reduction") has been suggested to explain the enhanced toxicity of other copper complexes compared to their free ligands by Kowol, *et al.* [41]. Protection from compound induced cell death by coadministration of the potent ROS scavenger NAC supports this theory. ROS production induced by the metal complexes of ligand **3** was supported by the ROS-sensitive DCFDA fluorescence assay.

5. Abbreviations

ABC	ATP-binding cassette
APT	attached proton test
ASC	L-ascorbic acid
CT	charge transfer
CV	cyclic voltammetry
DCFDA	2′,7′-dichlorofluorescin diacetate
DMEM	Dulbecco's Modified Eagle medium
EGFP	enhanced green fluorescent protein
ESI-MS	electrospray ionisation-mass spectrometry
GSH	glutathione
GSSG	glutathione disulfide
HEPES	4-(2-hydroxyethyl)-1-piperazineethanesulfonic acid
MDCK	Madin-Darby canine kidney
MDR	multidrug resistance
MES	2-(N-morpholino)ethanesulfonic acid
MTT	3-(4,5-dimethylthiazol-2-yl)-2,5-diphenyltetrazolium bromide
NAC	*N*-acetylcysteine
PBS	phosphate buffered saline
Pgp	P-glycoprotein
ROS	reactive oxygen species
RPMI	Roswell Park Memorial Institute
RR	ribonucleotide reductase
SB	Sleeping Beauty
TBACl	tetrabutylammonium chloride
THF	tetrahydrofuran

TQ Tariquidar

Acknowledgments

This research was supported by the Hungarian Research Foundation OTKA PD103905 and by the European Union and the State of Hungary co-financed by and the European Social Fund in the framework of TÁMOP-4.2.4.A/ 2-11/1-2012-0001 'National Excellence Program'. GS was supported by a Momentum Grant of the Hungarian Academy of Sciences. Funding from ERC (StG-260572) and NKTH-ANR 10-1-2011-0401 is also acknowledged.

References

[1] U. Jungwirth, C.R. Kowol, B.K. Keppler, C.G. Hartinger, W. Berger, P. Heffeter, Antioxid. Redox Signal. 15 (2011) 1085–1127.

[2] M. Valko, H. Morris, M.T.D. Cronin, Curr. Med. Chem. 12 (2005) 1161–1208.

[3] J.A. Jacobsen, J.L. Fullagar, M.T. Miller, S.M. Cohen, J. Med. Chem. 54 (2011) 591–602.

[4] R. McRae, P. Bagchi, S. Sumalekshmy, C.J. Fahrni, Chem. Rev. 109 (2009) 4780–4827.

[5] D.S. Kalinowski, Pharmacol. Rev. 57 (2005) 547–583.

[6] A. Budimir, Acta Pharm. 61 (2011) 1–14.

[7] A.M. Merlot, D.S. Kalinowski, D.R. Richardson, Antioxid. Redox Signal. 18 (2013) 973–1006.

[8] M. Whitnall, J. Howard, P. Ponka, D.R. Richardson, Proc. Natl. Acad. Sci. 103 (2006) 14901–14906.

[9] D.R. Richardson, P.C. Sharpe, D.B. Lovejoy, D. Senaratne, D.S. Kalinowski, M. Islam, et al., J. Med. Chem. 49 (2006) 6510–6521.

[10] D.R. Richardson, K. Milnes, Blood. 89 (1997) 3025–3038.

[11] E.M. Becker, D.B. Lovejoy, J.M. Greer, R. Watts, D.R. Richardson, Br. J. Pharmacol. 138 (2003) 819–830.

[12] M.T. Cocco, C. Congiu, V. Lilliu, V. Onnis, Bioorg. Med. Chem. 14 (2006) 366–372.

[13] J.K. Seydel, K.-J. Schaper, B. Clement, S. Rüsch-Gerdes, N. Reiling, S. Ehlers, WO2011/047814, 2011.

[14] J.G. Cory, D.L. Downes, A.H. Cory, K.J. Schaper, J.K. Seydel, Anticancer Res. 14 (1994) 875–879.

[15] J.K. Seydel, K.-J. Schaper, DE3716131A1, 1987.

[16] N.T.V. Le, D.R. Richardson, Biochim. Biophys. Acta BBA - Rev. Cancer. 1603 (2002) 31–46.

[17] H. Eklund, U. Uhlin, M. Färnegårdh, D.T. Logan, P. Nordlund, Prog. Biophys. Mol. Biol. 77 (2001) 177–268.

[18] C.R. Kowol, R. Berger, R. Eichinger, A. Roller, M.A. Jakupec, P.P. Schmidt, et al., J. Med. Chem. 50 (2007) 1254–1265.

[19] Y. Yu, J. Wong, D.B. Lovejoy, D.S. Kalinowski, D.R. Richardson, Clin. Cancer Res. 12 (2006) 6876–6883.

[20] C.M. Nutting, C.M.L. van Herpen, A.B. Miah, S.A. Bhide, J.-P. Machiels, J. Buter, et al., Ann. Oncol. 20 (2009) 1275–1279.

[21] G. Rappa, A. Lorico, M.-C. Liu, G.D. Kruh, A.H. Cory, J.G. Cory, et al., Biochem. Pharmacol. 54 (1997) 649–655.

[22] G. Szakács, J.K. Paterson, J.A. Ludwig, C. Booth-Genthe, M.M. Gottesman, Nat. Rev. Drug Discov. 5 (2006) 219–234.

[23] V. Sharma, D. Piwnica-Worms, Chem. Rev. 99 (1999) 2545–2560.

[24] M.A. Gaston, L.R.S. Dias, A.C.C. Freitas, A.L.P. Miranda, E.J. Barreiro, Pharm. Acta Helv. 71 (1996) 213–219.

[25] L. Savini, L. Chiasserini, A. Gaeta, C. Pellerano, Bioorg. Med. Chem. 10 (2002) 2193–2198.

[26] K.J. Schaper, J.K. Seydel, M. Rosenfeld, J. Kazda, Lepr. Rev. 57 Suppl 3 (1986) 254–264.

[27] W. Klinkhammer, H. Müller, C. Globisch, I.K. Pajeva, M. Wiese, Bioorg. Med. Chem. 17 (2009) 2524–2535.

[28] G.R. Fulmer, A.J.M. Miller, N.H. Sherden, H.E. Gottlieb, A. Nudelman, B.M. Stoltz, et al., Organometallics. 29 (2010) 2176–2179.

[29] H.M. Irving, M.G. Miles, L.D. Pettit, Anal. Chim. Acta. 38 (1967) 475–488.

[30] Royal Society of Chemistry, SCQuery, The IUPAC Stability Constants Database, Academic Software, 2005.

[31] L. Zékány, I. Nagypál, in: D.L. Leggett (Ed.), Comput. Methods Determ. Stab. Constants, Plenum Press, New York, 1985: pp. 291–353.

[32] C.F. Baes, R.E. Mesmer, The Hydrolysis of Cations, Wiley, New York, 1976.

[33] A.J. Bard, L.R. Faulkner, Electrochemical Methods–Fundamentals and Applications, John Wiley & Sons, New York, 2000.

[34] L. Mátés, M.K.L. Chuah, E. Belay, B. Jerchow, N. Manoj, A. Acosta-Sanchez, et al., Nat. Genet. 41 (2009) 753–761.

[35] G. Szakács, C. Ozvegy, E. Bakos, B. Sarkadi, A. Váradi, Biochem. Biophys. Res. Commun. 276 (2000) 1314–1319.

[36] O. Kolacsek, V. Krízsik, A. Schamberger, Z. Erdei, A. Apáti, G. Várady, et al., Mob. DNA. 2 (2011) 5.

[37] G. Szakacs, C. Ozvegy, E. Bakos, B. Sarkadi, A. Varadi, Biochem J. 356 (2001) 71–5.

[38] K. Juvale, V.F.S. Pape, M. Wiese, Bioorg. Med. Chem. 20 (2012) 346–355.

[39] H. Mueller, M.U. Kassack, M. Wiese, J. Biomol. Screen. 9 (2004) 506–515.

[40] I. GraphPad Software, GraphPad Prism, GraphPad Software, Inc., 2007. www.graphpad.com.

[41] C.R. Kowol, P. Heffeter, W. Miklos, L. Gille, R. Trondl, L. Cappellacci, et al., J. Biol. Inorg. Chem. 17 (2012) 409–423.

[42] W.A. Morgan, B. Kaler, P.H. Bach, Toxicol. Lett. 94 (1998) 209–215.

[43] T. Ohashi, A. Mizutani, A. Murakami, S. Kojo, T. Ishii, S. Taketani, FEBS Lett. 511 (2002) 21–27.

[44] P.S. Kalsi, B.R. Chhabra, J. Singh, R. Vig, Synlett. 1992 (1992) 425–426.

[45] K.C. Agrawal, P.D. Mooney, A.C. Sartorelli, J. Med. Chem. 19 (1976) 970–972.

[46] B.R. Chhabra, K. Hayano, T. Ohtsuka, H. Shirahama, T. Matsumoto, Chem. Lett. 10 (1981) 1703–1706.

[47] Y. Tagawa, K. Yamashita, Y. Higuchi, Y. Goto, Heterocycles. 60 (2003) 953–957.

[48] L. ChemAxon, MarvinSketch, ChemAxon Ltd., Budapest, Hungary, 2012. http://www.chemaxon.com.

[49] E. Rutkowska, K. Pajak, K. Jóźwiak, Acta Pol. Pharm. 70 (2013) 3–18.

[50] M. Bakker, J. Renes, A. Groenhuijzen, P. Visser, H. Timmer-Bosscha, M. Müller, et al., Int. J. Cancer. 73 (1997) 362–366.

[51] W.G. Harker, B.I. Sikic, Cancer Res. 45 (1985) 4091–4096.

[52] D.-W. Shen, C. Cardarelli, J. Hwang, M. Cornwell, N. Richert, S. Ishii, et al., J. Biol. Chem. 261 (1986) 7762–7770.

[53] É.A. Enyedy, N.V. Nagy, É. Zsigó, C.R. Kowol, V.B. Arion, B.K. Keppler, et al., Eur. J. Inorg. Chem. 2010 (2010).

[54] D.B. Lovejoy, P.J. Jansson, U.T. Brunk, J. Wong, P. Ponka, D.R. Richardson, Cancer Res. 71 (2011) 5871–5880.

[55] R.J. Motekaitis, R.M. Smith, A.E. Martell, Critically Selected Stability Constants of Metal Complexes Database, College Station, TX, USA, 1997.

[56] R.J. Motekaitis, A.E. Martell, Inorganica Chim. Acta. 183 (1991) 71–80.

[57] E.T. Clarke, A.E. Martell, Inorganica Chim. Acta. 196 (1992) 185–194.

[58] É.A. Enyedy, M.F. Primik, C.R. Kowol, V.B. Arion, T. Kiss, B.K. Keppler, Dalton Trans. 40 (2011) 5895.

[59] R. Bendre, A. Murugkar, S. Padhye, P. Kulkarni, M. Karve, Met.-Based Drugs. 5 (1998) 59–66.

[60] G. Szakács, M.D. Hall, M.M. Gottesman, A. Boumendjel, R. Kachadourian, B.J. Day, et al., Chem. Rev. (2014) 5753-5774.

[61] A.-M. Albrecht-Gary, A.L. Crumbliss, Coordination Chemistry of Siderophores: Thermodynamics and Kinetics of iron chelation and release, in: A. Sigel, H. Sigel (Eds.), Met. Ions Biol. Syst., Marcel Dekker, Inc., New York, 1998: pp. 239–328.

[62] F.Q. Schafer, G.R. Buettner, Free Radic. Biol. Med. 30 (2001) 1191–1212.

[63] T. Jakusch, É.A. Enyedy, K. Kozma, Z. Paár, A. Bényei, T. Kiss, Inorganica Chim. Acta. 420 (2014) 92–102.

[64] B. Song, N. Aebischer, C. Orvig, Inorg. Chem. 41 (2002) 1357–1364.

[65] C.G. Hartinger, S. Zorbas-Seifried, M.A. Jakupec, B. Kynast, H. Zorbas, B.K. Keppler, J. Inorg. Biochem. 100 (2006) 891–904.

[66] J.J. Ruiz, A. Aldaz, M. Dominguez, Can. J. Chem. 55 (1977) 2799–2806.

[67] A. Gomes, E. Fernandes, J.L.F.C. Lima, J. Biochem. Biophys. Methods. 65 (2005) 45–80.

[68] B. Kalyanaraman, V. Darley-Usmar, K.J.A. Davies, P.A. Dennery, H.J. Forman, M.B. Grisham, et al., Free Radic. Biol. Med. 52 (2012) 1–6.

[69] D. Türk, M.D. Hall, B.F. Chu, J.A. Ludwig, H.M. Fales, M.M. Gottesman, et al., Cancer Res. 69 (2009) 8293–8301.

[70] O. Polgar, S.E. Bates, Biochem. Soc. Trans. 33 (2005) 241–246.

[71] G. Szakács, G.K. Chen, M.M. Gottesman, Cancer Biol. Ther. 3 (2004) 382–384.

[72] A. Tamaki, C. Ierano, G. Szakacs, R.W. Robey, S.E. Bates, Essays Biochem. 50 (2011) 209–232.

[73] V. Jekerle, W. Klinkhammer, R.M. Reilly, M. Piquette-Miller, M. Wiese, Cancer Chemother. Pharmacol. 59 (2006) 61–69.

[74] P. Mistry, A.J. Stewart, W. Dangerfield, S. Okiji, C. Liddle, D. Bootle, et al., Cancer Res. 61 (2001) 749–758.

[75] L. Amiri-Kordestani, A. Basseville, K. Kurdziel, A.T. Fojo, S.E. Bates, Drug Resist. Updat. 15 (2012) 50–61.

[76] M. Falasca, K.J. Linton, Expert Opin. Investig. Drugs. 21 (2012) 657–666.

[77] M. Yu, A. Ocana, I.F. Tannock, Cancer Metastasis Rev. 32 (2013) 211–227.

[78] G. Szakács, J.-P. Annereau, S. Lababidi, U. Shankavaram, A. Arciello, K.J. Bussey, et al., Cancer Cell. 6 (2004) 129–137.

Legends to the Schemes and Figures

Scheme 1 Synthetic routes for the pyrimidinylhydrazones **1, 2** and **3** starting from commercially available 4,6-dichloropyrimidine (1193-21-1) and 5-ethyl-2-methyl-pyridine (104-90-5). Reaction conditions were as follows a) NaH, methanol, -10 °C to RT; b) N_2H_4, methanol, 65 °C; c) H_2O_2, glacial acetic acid, 120 °C; d) acetic anhydride, glacial acetic acid, 120 °C; e) NaOH, THF, 70 °C; f) freshly prepared MnO_2, $CHCl_3$, ultrasound, 50 °C; g) catalytic acetic acid, ethanol, 80 °C .

Scheme 2 Protonation and deprotonation equilibria for ligand **3**.

Fig. 1 UV-Vis absorption spectra of ligand **3** recorded at different pH values (a), calculated individual absorption spectra (b) and concentration distribution curves for ligand species (c). *{c_{ligand} = 50 μM; t = 25.0 °C, I = 0.20 M (KCl)}.*

Fig. 2 UV–Vis absorption spectra recorded for the Fe(III) - ligand **3** system at various pH values and at 1:2 metal-to-ligand ratio. *Inset shows the pH-dependent absorbance values at 420 nm for the same system (●) and for the ligand alone (♦). {c_{ligand} = 50 μM; t = 25.0 °C, I = 0.20 M (KCl)}.*

Fig. 3 UV–Vis absorption spectra recorded for the Cu(II) - ligand **3** system at various pH values and at 1:1 metal-to-ligand ratio (a) and calculated individual absorption spectra of the Cu(II) complexes (b). *{c_{ligand} = 50 μM; t = 25.0 °C, I = 0.20 M (KCl)}.*

Fig. 4 Toxicity of ligand **3** assessed in the presence of increasing concentrations of $FeCl_3$ (a) or $CuCl_2$ (b) in MES-SA (open squares) and MES-SA-Dx5 (filled squares) cells. IC_{50} values were obtained after 72 h incubation with the compounds, measured by the MTT assay. Data represent the mean standard deviation obtained in 6 (a) and 3 (b) independent experiments.

Fig. 5 Cyclic voltammograms of iron (a) and copper (b) complexes of ligand **3** *vs.* Ag/AgCl/KCl (1.0 M) *{t = 25.0 °C, I =0.01 M (TBACl) in 90% (v/v) DMSO/H_2O mixture, c_L =1.0 mM; 100 mV/s scan rate, glassy carbon working electrode}.* Data obtained with the ligand alone (dashed, grey) or at various M:L ratios (1:0 (dashed dotted black, 1:1 (solid red), 1:2 (dotted blue) and 1:3 (solid green)) are shown.

Fig. 6 Time-dependent UV–Vis spectra of Cu(II) – ligand **3** – ASC (a) and GSH (c), as well as Fe(III) – ligand **3** – ASC (b) and GSH (d) system at 1:1:10 ratio. The red line denotes the spectrum obtained upon addition of H_2O_2. *{$c_{Cu(II)}$ = 25 μM; $c_{Fe(III)}$ = 50 μM; t = 25.0 °C, I= 0.1 M (KCl); pH 7.40 (50 mM HEPES) for the Cu(II) and pH 5.45 (50 mM MES) for the Fe(III) complexes}.*

Fig. 7 Effect of the antioxidant scavenger NAC on the toxicity of **3.** A2780 (a) or A2780adr (b) cells were treated with increasing amounts of **3** with or without the ROS scavenger NAC. Dose response curves obtained for **3** alone (black circles) or in the presence of 1 mM (green circles), 2.5 mM (red diamonds) and 5 mM (blue squares) of NAC are shown. Data represent at least three independent experiments with standard deviation. (c) depicts IC50 values of ligand **3** and its copper (II) complexes obtained in MESSA (open columns) and MESSA-Dx5 (filled columns) cells in presence or absence of 5 mM NAC. Asterisks indicate significance as calculated from t-tests (*: $p < 0.05$, **: $p < 0.005$, *** $p < 0.0005$).

Fig. 8 Characterization of intracellular ROS production with the DCFDA assay. ROS induction by 50 μM or 100 μM ligand **3** was evaluated in the presence of equimolar and half equimolar amount of Fe(III) (a) or Cu(II) (b). MES-SA cells (open columns) were loaded with DCFDA and fluorescence intensity was measured following 80 min incubation with the indicated compounds. As a control the signal induced with 1.6 mM tert-butyl hydroperoxide is shown. Dotted columns represent the cell-free condition (the interaction between the dye and the tested compounds). Fold change in fluorescence represents the ratio of the measured fluorescence intensity to the basal intensity before treatment with

the indicated compounds. Values show the mean of five independent experiments performed in duplicates; error bars represent standard deviation.

Fig. 9 Effect of Pgp-inhibition on the toxicity of ligand **3**. A2780 and A2780adr (a) or MES-SA and MES-SADx5 (b) cells were treated with increasing amounts of **3**. Open symbols represent the drug-sensitive parental lines; filled symbols represent the Pgp-expressing MDR derivatives. The effect of the Pgp inhibitors WK-X-24 for A2780adr, and TQ for MES-SADx5 is shown with grey symbols.

Fig. 10 Intracellular redox reactions involved in the redox cycling of metal ions. Green arrows depict reactions catalyzed by the copper-containing superoxide dismutase enzyme [41], the red arrow represents the Fenton reaction [1]; the blue arrows represent the redox cycling of the metal ions, which can be activated by the reduction through antioxidants such as glutathione or NAC.

Synthesis and characterization of the anticancer and metal binding properties of novel pyrimidinylhydrazone derivatives

Veronika F.S. Pape[a,b], Dóra Türk[a], Pál Szabó[c], Michael Wiese[b], Eva A. Enyedy[d,*], Gergely Szakács[a,*]

[a] *Institute of Enzymology, Research Centre for Natural Sciences, Hungarian Academy of Sciences, Magyar Tudósok körútja 2, H-1117 Budapest, Hungary*

[b] *Department of Pharmaceutical Chemistry, University of Bonn, An der Immenburg 4, D-53121 Bonn, Germany*

[c] *Institute of Organic Chemistry, Research Centre for Natural Sciences, Hungarian Academy of Sciences, Magyar Tudósok körútja 2, H-1117 Budapest, Hungary*

[d] *Department of Inorganic and Analytical Chemistry, University of Szeged, Dóm tér 7. H-6720 Szeged, Hungary*

Table 1 Characterization of the relative lipophilicity of compounds **1**, **2** and **3**. Calculations were performed with MarvinSketch 5.9.0 ($\log D_{7.4}$). [48]; log K_w values were obtained by HPLC-MSMS.

	1	**2**	**3**
$\log D_{7.4}$	2.36	3.32	1.92
log K_w	2.42	3.49	2.67

Table 2 Cytotoxicity of the synthesized pyrimidinylhydrazones measured with MTT viability assay after 72 h of incubation. Values represent the mean +/- standard deviation of IC_{50} values (μM) obtained in at least three independent experiments.

IC_{50} (μM)±SD	**1**	**2**	**3**
A2780	1.69 ± 0.60	1.31 ± 0.26	0.14 ± 0.05
A2780adr	1.97 ± 0.11	0.64 ± 0.14	0.03 ± 0.01
KB-3-1	1.96 ± 0.43	1.23 ± 0.04	0.35 ± 0.07
KB-v1	2.84 ± 0.60	1.58 ± 0.33	0.51 ± 0.14
MES-SA	2.84 ± 0.32	1.39 ± 0.32	0.31 ± 0.15
MES-SA-Dx5	2.54 ± 0.98	1.06 ± 0.27	0.13 ± 0.07
MDCK	6.30 ± 2.21	1.84 ± 0.97	0.51 ± 0.48
MDCK-ABCB1	3.55 ± 0.64	1.25 ± 0.74	0.29 ± 0.03

Table 3. Overall protonation ($\log\beta(H_iL)$) and proton dissociation constants (pK_a) of ligand **3** together with the λ_{max} (nm) / ε ($M^{-1}cm^{-1}$) values of the individual species *{t = 25.0 °C, I = 0.20 M (KCl)}*.

	$\log\beta(H_iL)$	pK_a	λ_{max} (nm)	ε ($M^{-1}cm^{-1}$)
L		-	312	20198
HL^+	4.60±0.01	4.60 (pK_2)	282	10650
			356	17520
H_2L^{2+}	6.89±0.01	2.29 (pK_1)	276	10560
			344	23340

Table 4 Overall stability and stepwise constants of Fe(III) and Cu(II) complexes of ligand **3** together with the λ_{max} (nm) / ε ($M^{-1}cm^{-1}$) values of the individual species *{t = 25.0 °C, I = 0.20 M (KCl)}*.

	Fe(III)				Cu(II)			
	n	**logβ**	λ_{max} (nm)	ε ($M^{-1}cm^{-1}$)	n	**logβ**	λ_{max} (nm)	ε ($M^{-1}cm^{-1}$)
$[MLH]^{n+}$	-	-	-	-	3	12.16±0.09	342	16640
$[ML]^{n+}$	3	15.69±0.07	320 368 424	10600 10800 8600	2	7.39±0.01	410	19600
$[ML_2]^{n+}$	3	21.71±0.06	380 304	12500 9200	2	12.35±0.03	402	40510
logK_2		6.02				4.96		

Scheme 1

Click here to download high resolution image

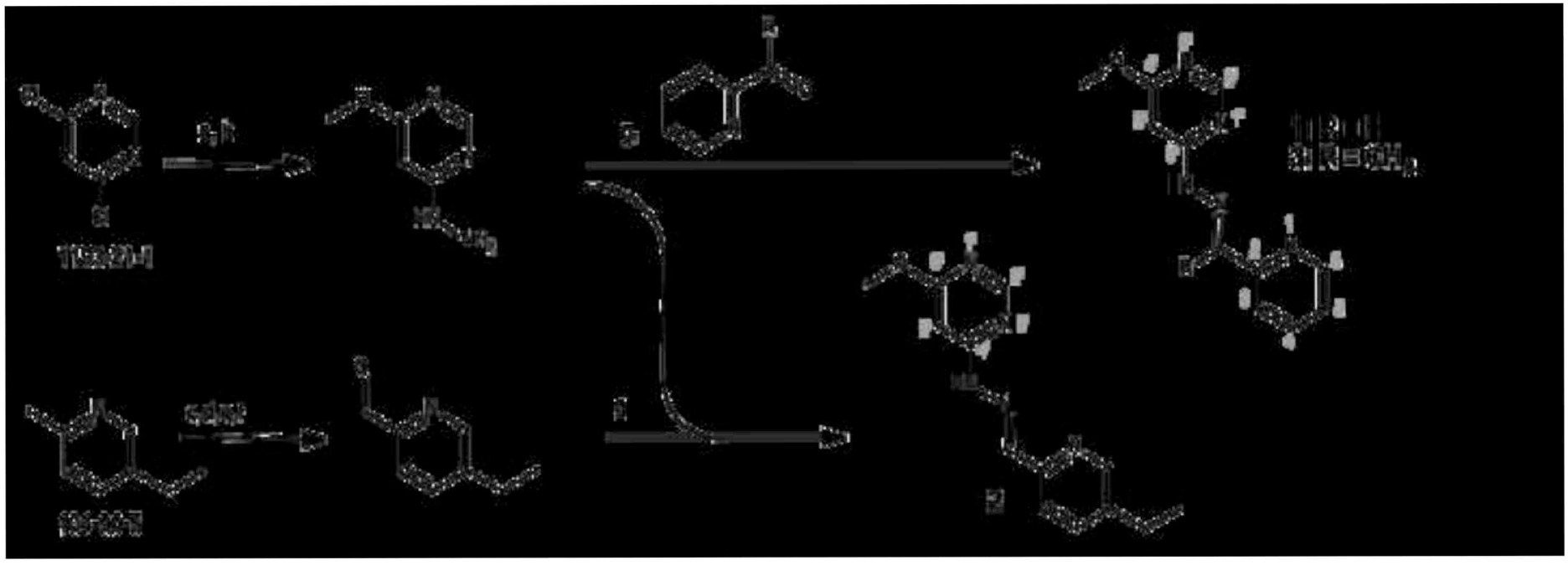

Scheme 2

Click here to download high resolution image

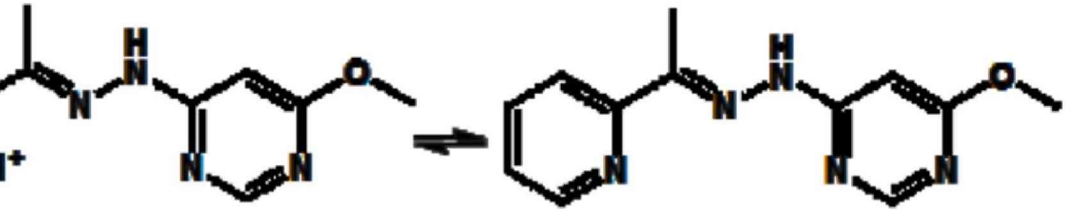
HL+
L

Figure 1
Click here to download high resolution image

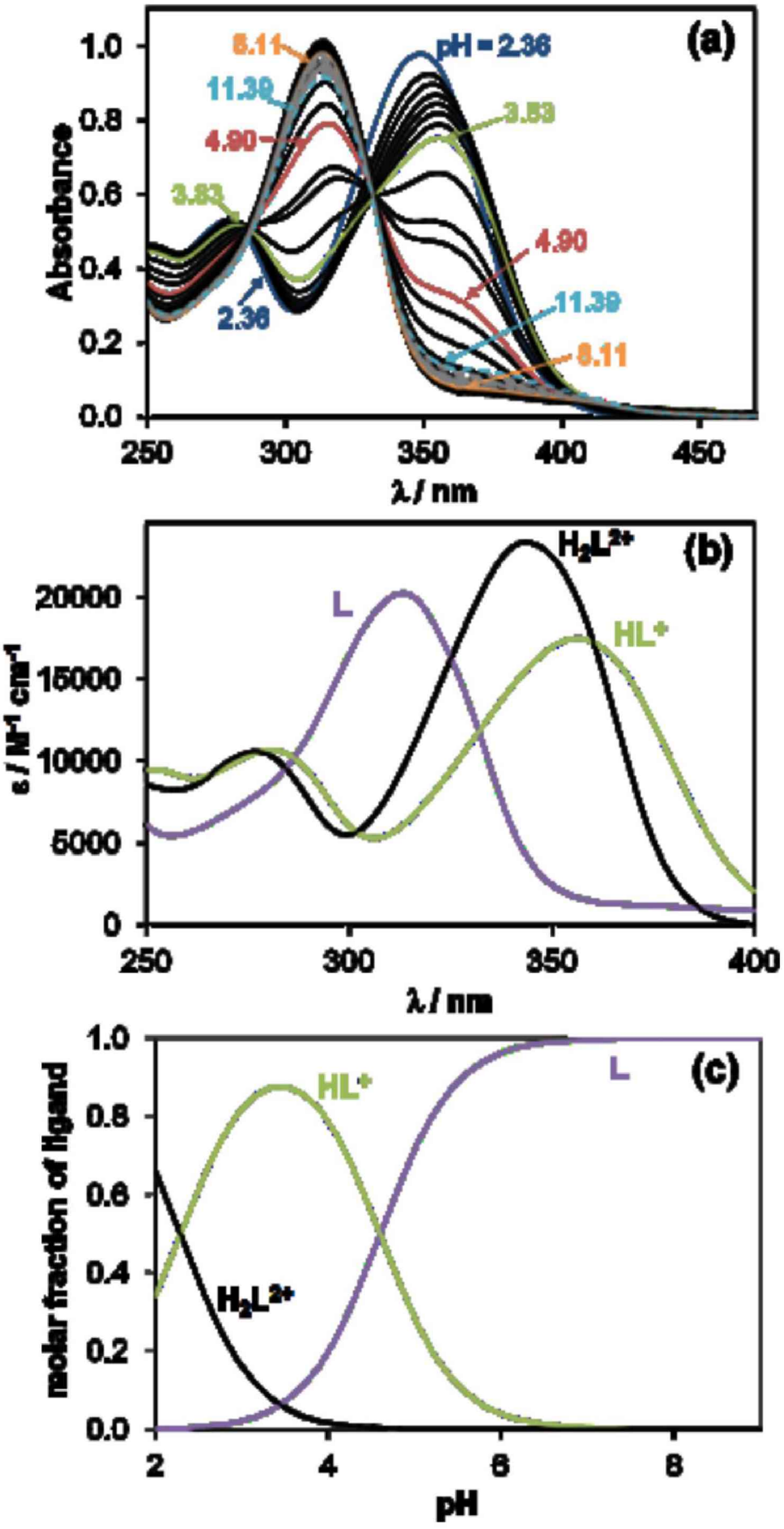

Figure 2
Click here to download high resolution image

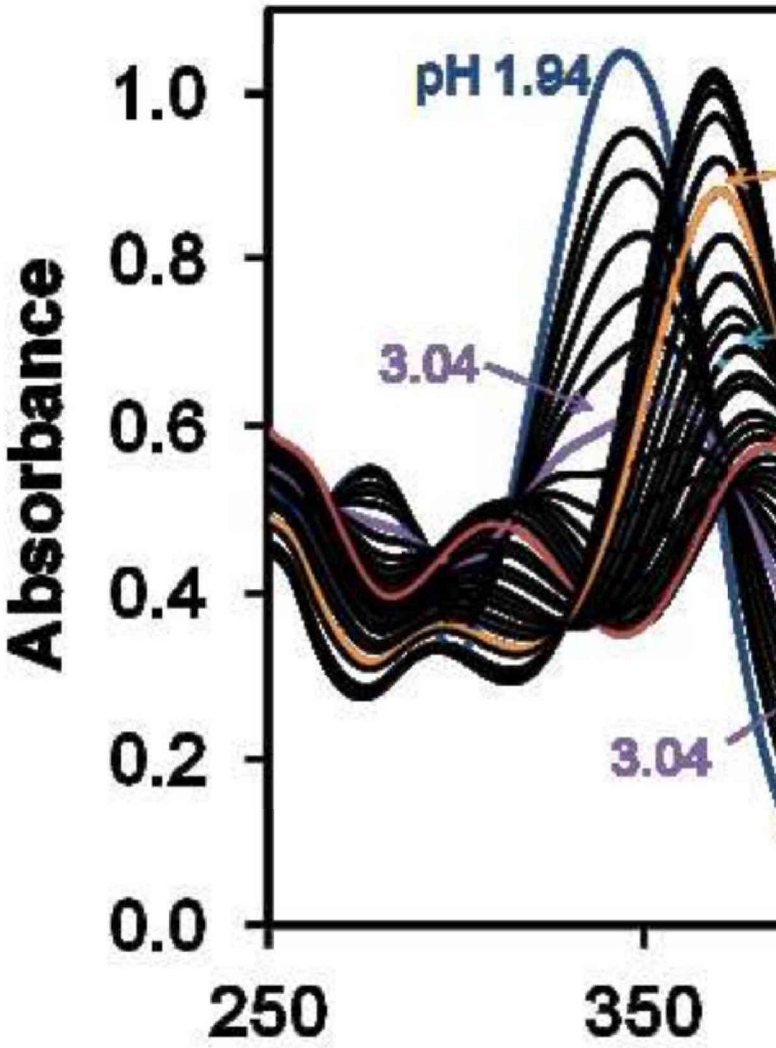

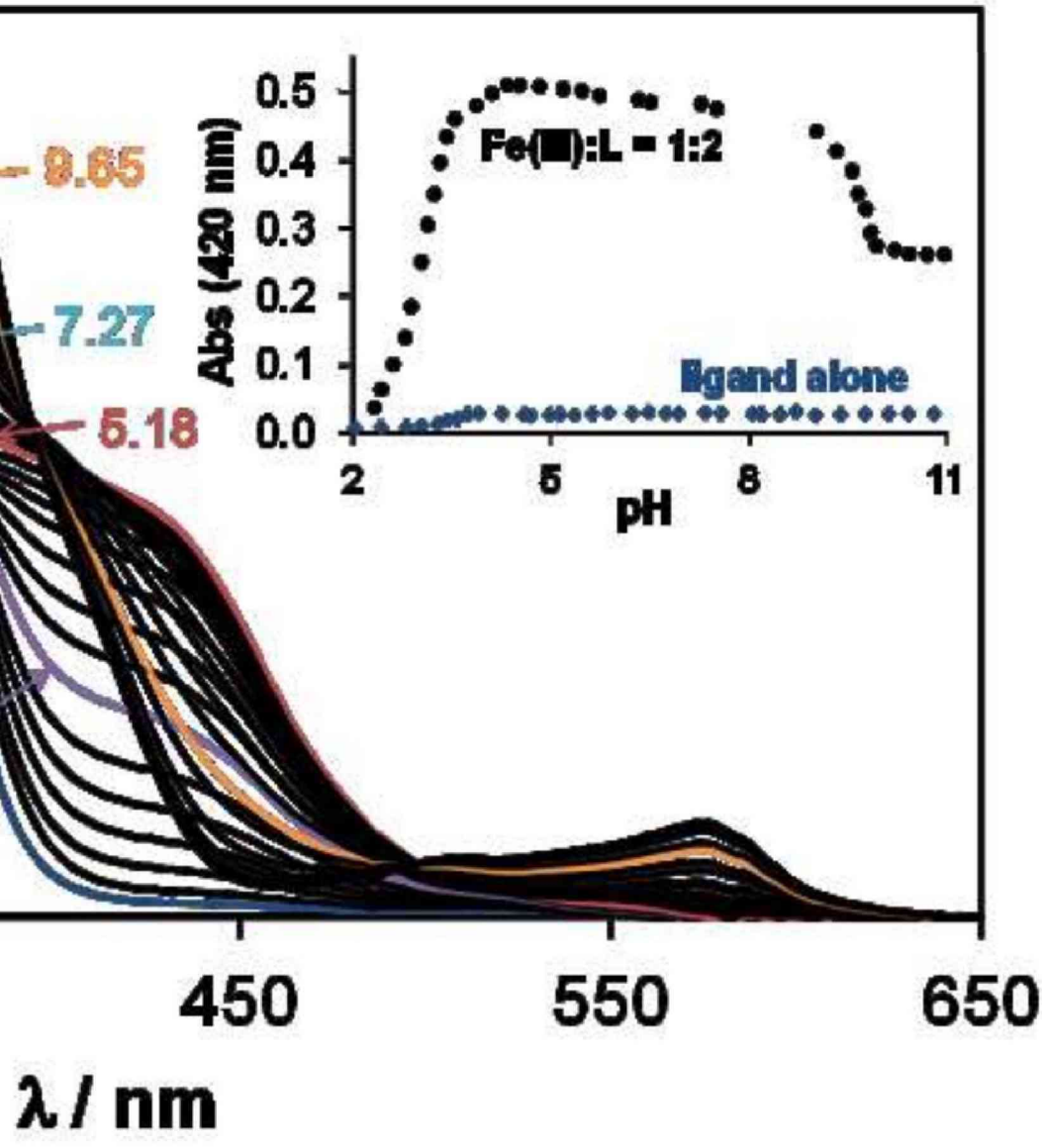
9.65
7.27
5.18
Abs (420 nm)
0.5
0.4
0.3
0.2
0.1
0.0
Fe(III):L = 1:2
ligand alone
2
5
8
11
pH
450
550
650
λ / nm

Figure 3
Click here to download high resolution image

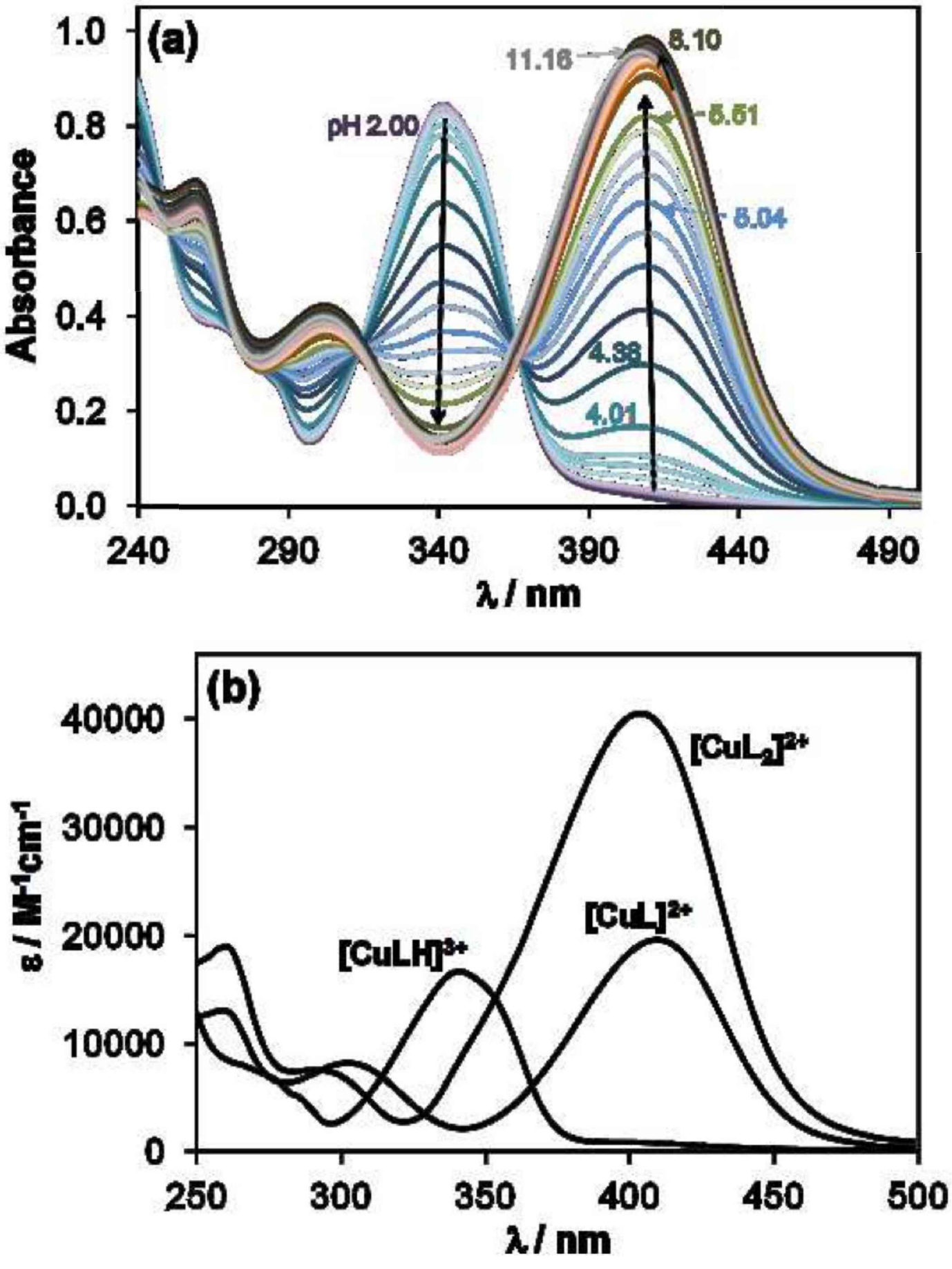

Figure 4
Click here to download high resolution image

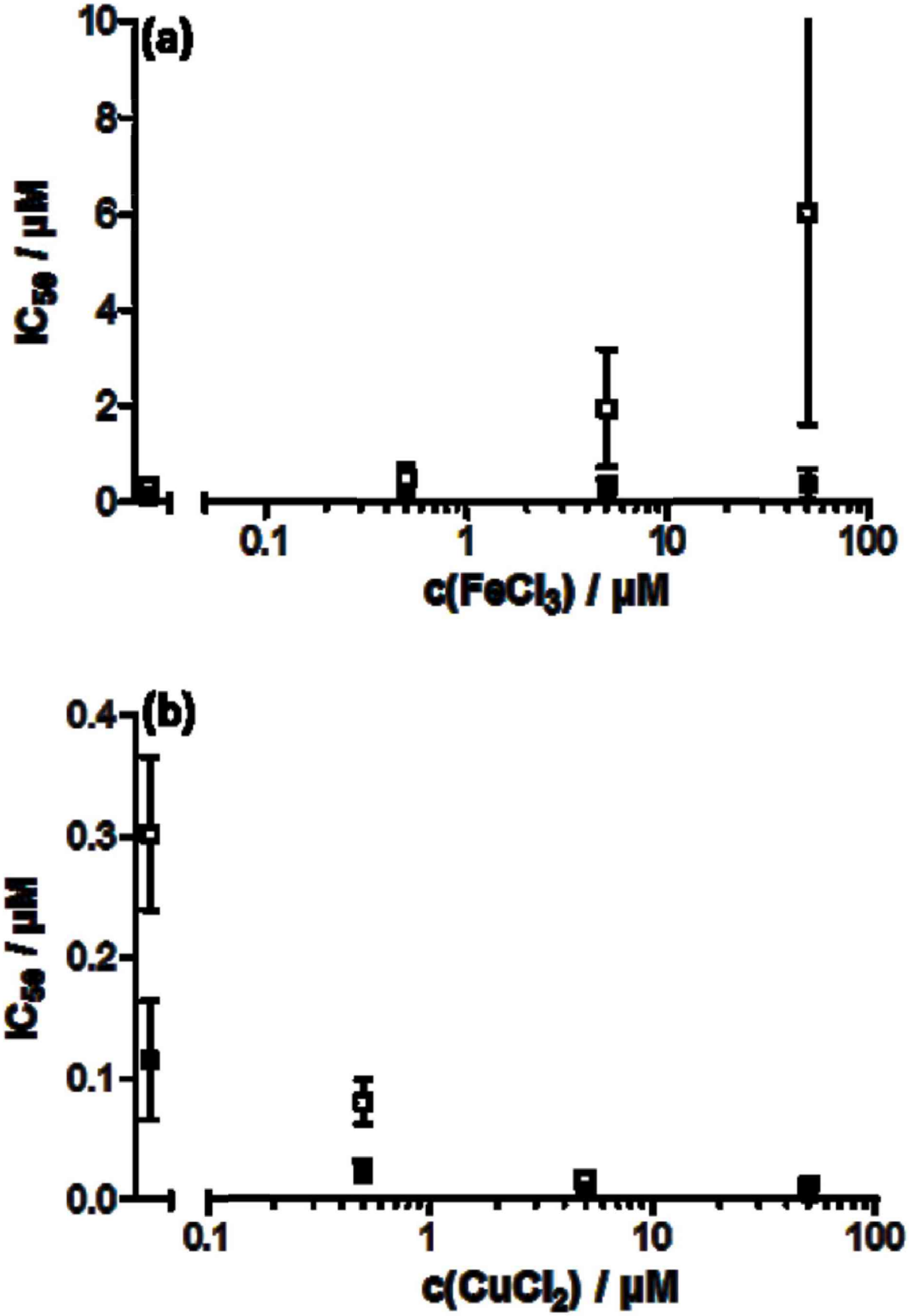

Figure 5
Click here to download high resolution image

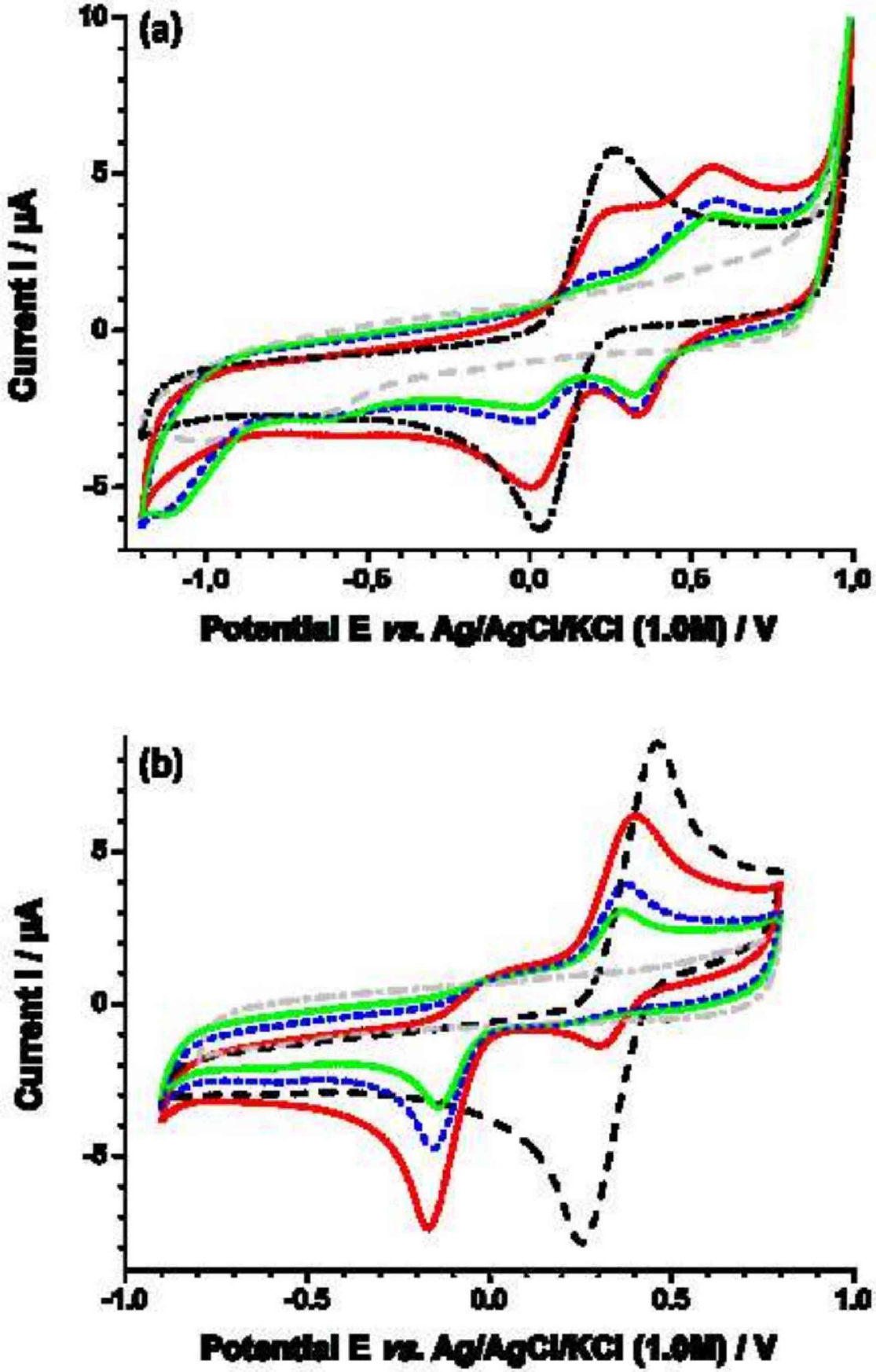

Figure 6
Click here to download high resolution image

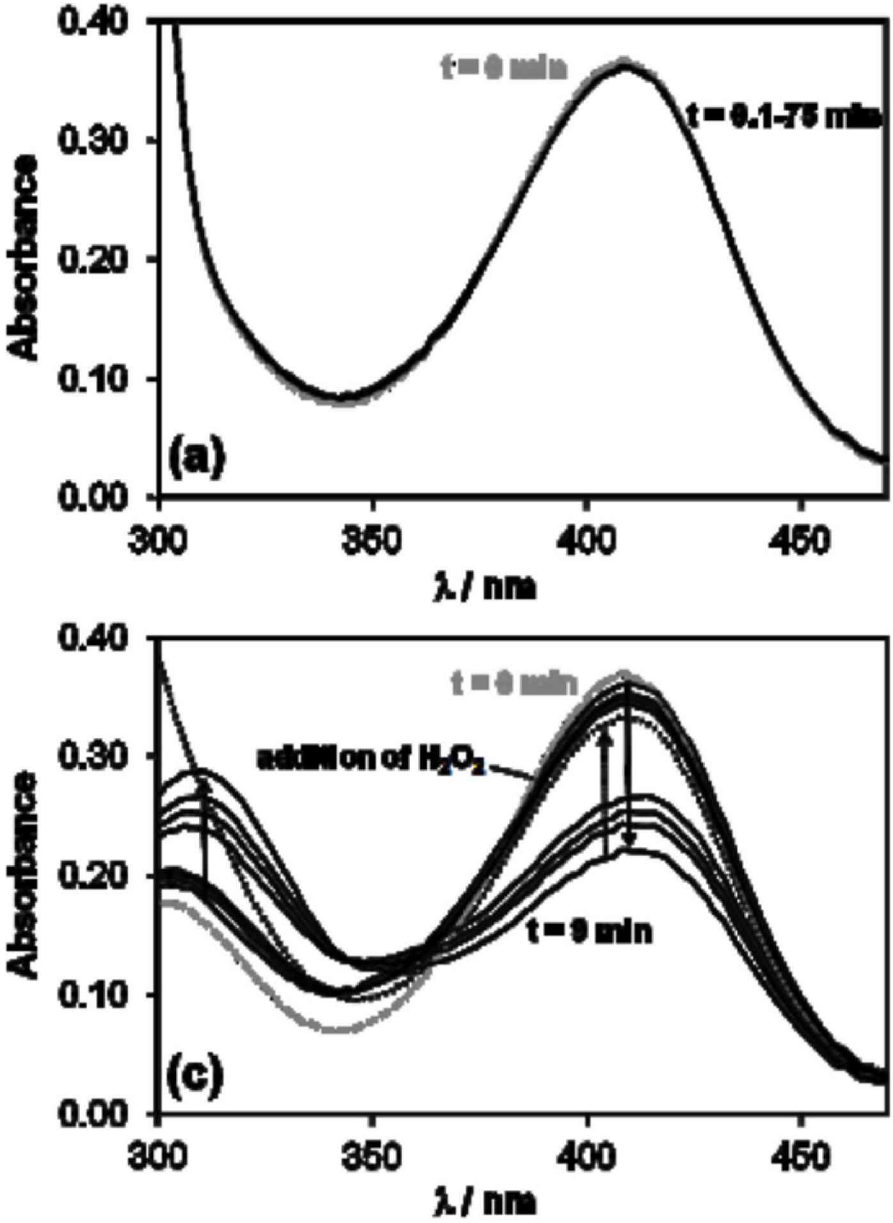

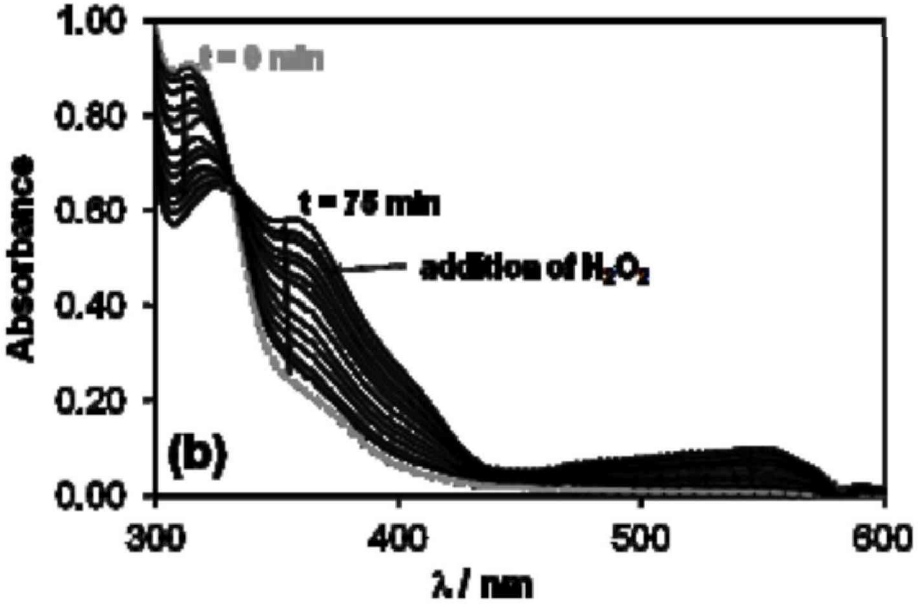
1.00
0.80
0.60
0.40
0.20
0.00
Absorbance
t = 0 min
t = 75 min
addition of H_2O_2
(b)
300
400
500
600
λ / nm

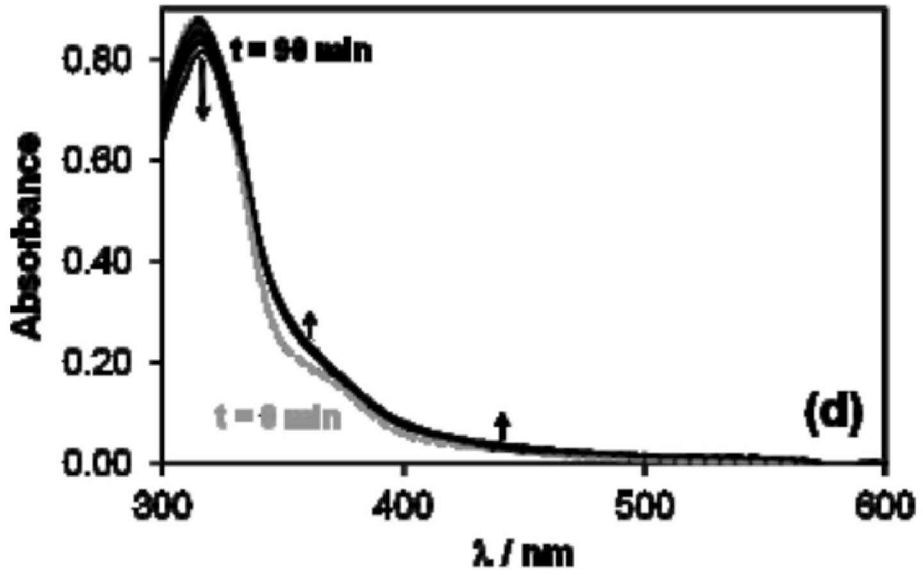
0.80
0.60
0.40
0.20
0.00
Absorbance
t = 90 min
t = 0 min
(d)
300
400
500
600
λ / nm

Figure 7
Click here to download high resolution image

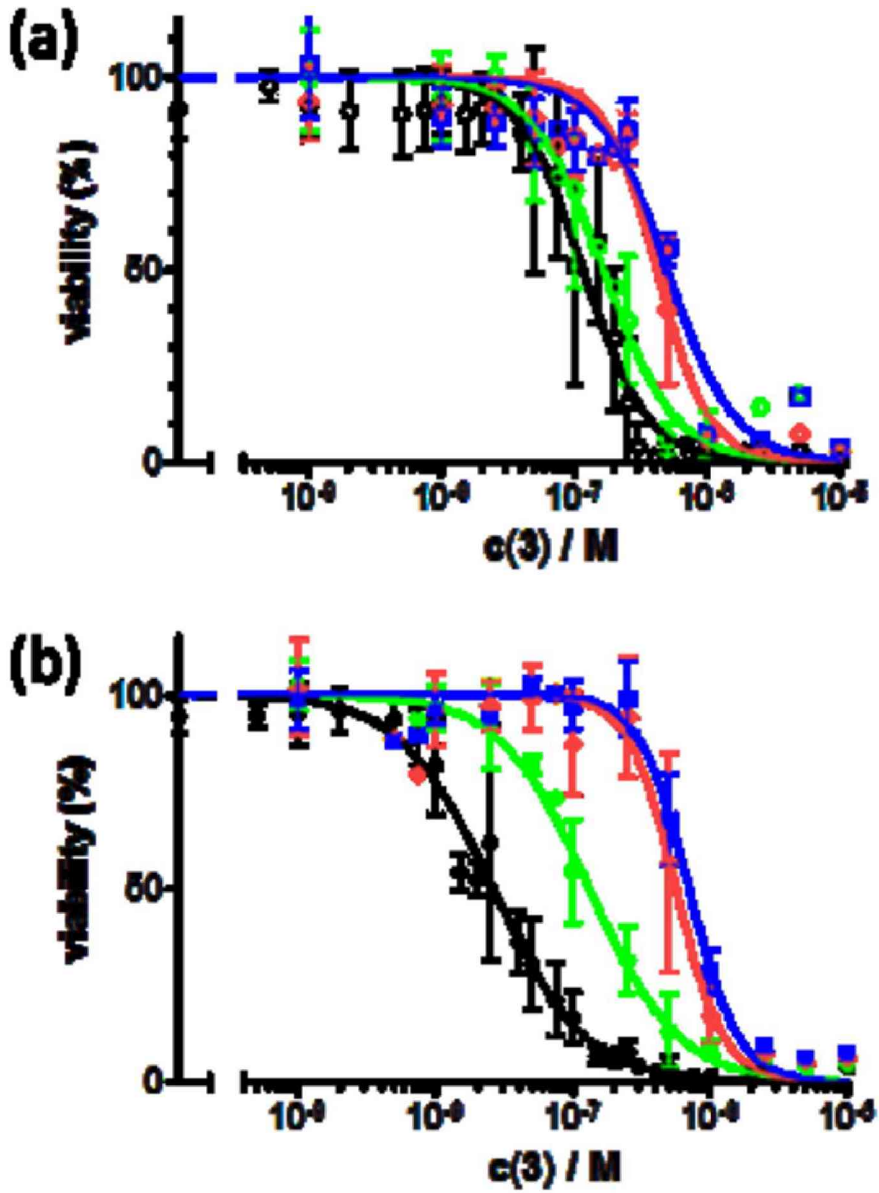

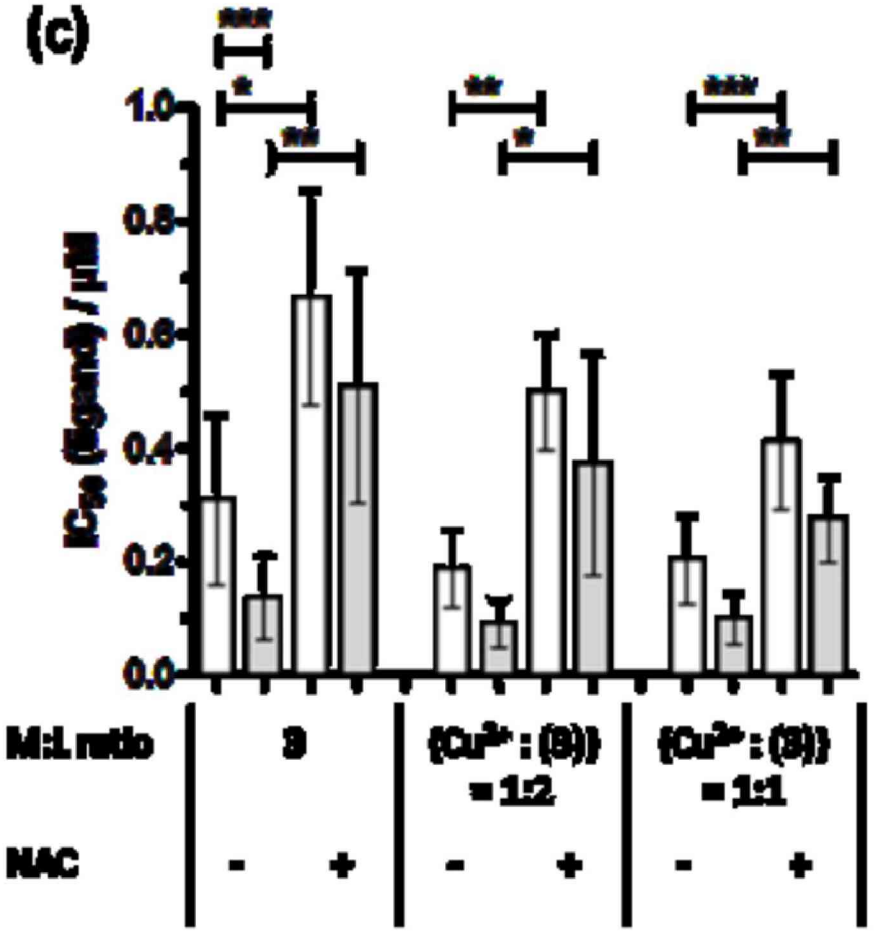
(c)
***
*
**
**
*
***
*
**
1.0
0.8
0.6
0.4
0.2
0.0
IC50 (ligand) / μM
M:L ratio
3
(Cu2+ : (3)) = 1:2
(Cu2+ : (3)) = 1:1
NAC
-
+
-
+
-
+

Figure 8
Click here to download high resolution image

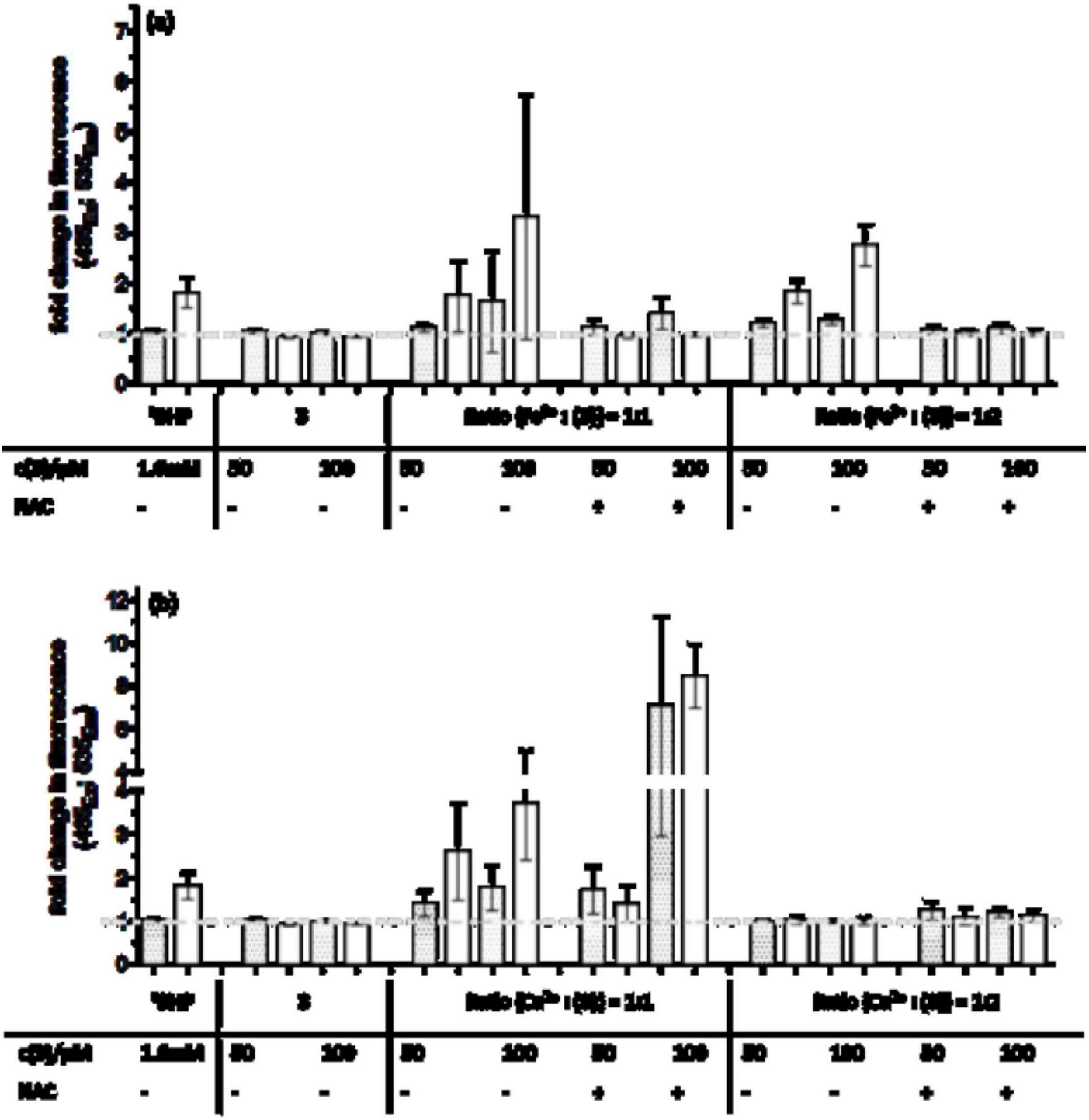

Figure 9
Click here to download high resolution image

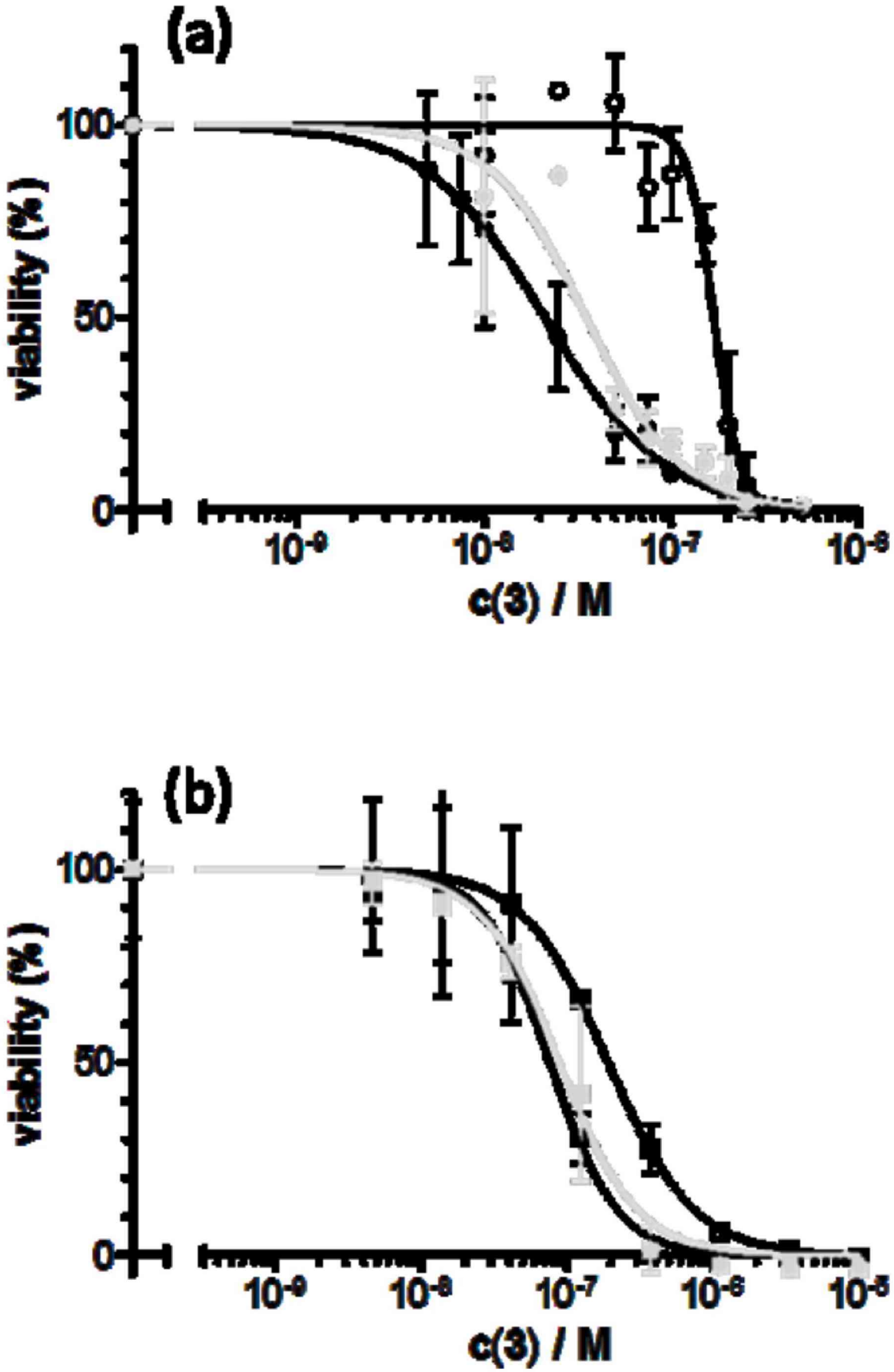

Figure 10
Click here to download high resolution image

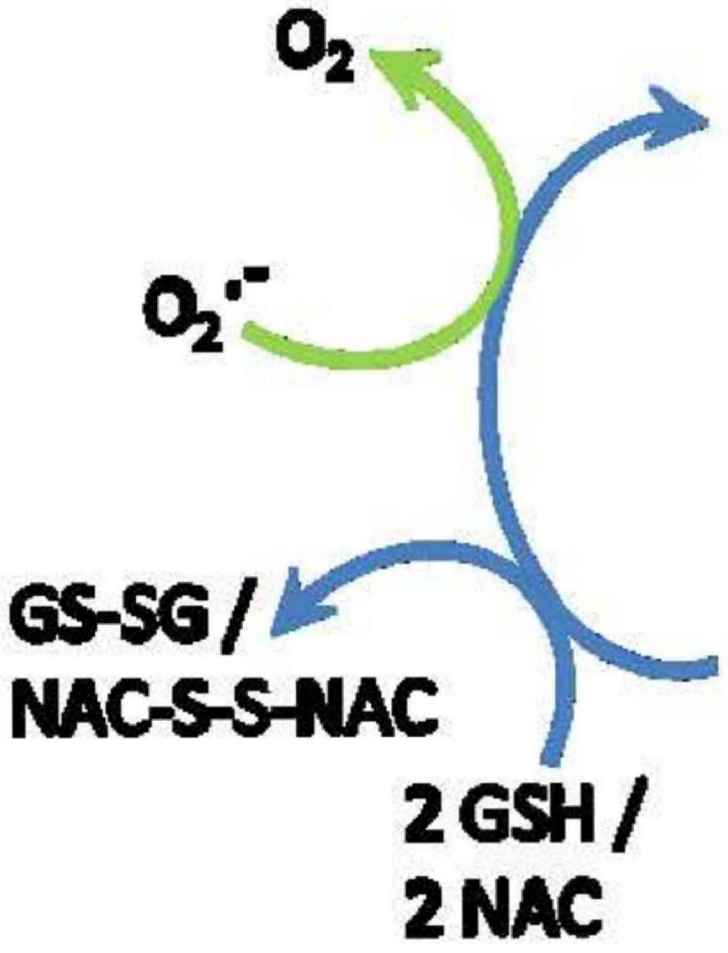

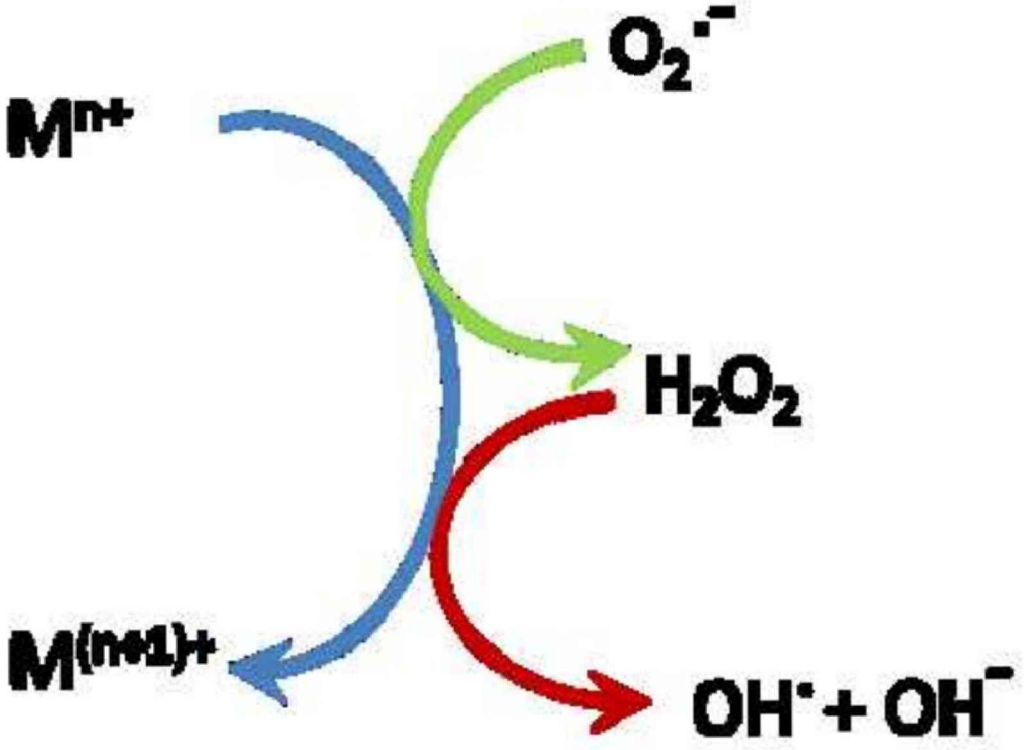
$O_2^{\bullet-}$
M^{n+}
H_2O_2
$M^{(n+1)+}$
$OH^{\bullet} + OH^-$

Supplementary Information for Publication Online

Click here to download Supplementary Information for Publication Online: Pape JIB Supp 2014.11.03..docx

Supplementary Fig 1

Click here to download Supplementary Information for Publication Online: Fig A1.tif

Suppl Fig A2

Click here to download Supplementary Information for Publication Online: Fig A2.tif

Suppl Fig A3

Click here to download Supplementary Information for Publication Online: Fig A3.tif

Supplementary Fig 4

Click here to download Supplementary Information for Publication Online: Fig A4.tif